NASA/TM—2007–215189

Modeling of Turbulence Effect on Liquid Jet Atomization

H.P. Trinh
Marshall Space Flight Center, Marshall Space Flight Center, Alabama

December 2007

The NASA STI Program…in Profile

Since its founding, NASA has been dedicated to the advancement of aeronautics and space science. The NASA Scientific and Technical Information (STI) Program Office plays a key part in helping NASA maintain this important role.

The NASA STI program operates under the auspices of the Agency Chief Information Officer. It collects, organizes, provides for archiving, and disseminates NASA's STI. The NASA STI program provides access to the NASA Aeronautics and Space Database and its public interface, the NASA Technical Report Server, thus providing one of the largest collections of aeronautical and space science STI in the world. Results are published in both non-NASA channels and by NASA in the NASA STI Report Series, which includes the following report types:

- TECHNICAL PUBLICATION. Reports of completed research or a major significant phase of research that present the results of NASA programs and include extensive data or theoretical analysis. Includes compilations of significant scientific and technical data and information deemed to be of continuing reference value. NASA's counterpart of peer-reviewed formal professional papers but has less stringent limitations on manuscript length and extent of graphic presentations.

- TECHNICAL MEMORANDUM. Scientific and technical findings that are preliminary or of specialized interest, e.g., quick release reports, working papers, and bibliographies that contain minimal annotation. Does not contain extensive analysis.

- CONTRACTOR REPORT. Scientific and technical findings by NASA-sponsored contractors and grantees.

- CONFERENCE PUBLICATION. Collected papers from scientific and technical conferences, symposia, seminars, or other meetings sponsored or cosponsored by NASA.

- SPECIAL PUBLICATION. Scientific, technical, or historical information from NASA programs, projects, and missions, often concerned with subjects having substantial public interest.

- TECHNICAL TRANSLATION. English-language translations of foreign scientific and technical material pertinent to NASA's mission.

Specialized services also include creating custom thesauri, building customized databases, and organizing and publishing research results.

For more information about the NASA STI program, see the following:

- Access the NASA STI program home page at <http://www.sti.nasa.gov>

- E-mail your question via the Internet to <help@sti.nasa.gov>

- Fax your question to the NASA STI Help Desk at 301–621–0134

- Phone the NASA STI Help Desk at 301–621–0390

- Write to:
  NASA STI Help Desk
  NASA Center for AeroSpace Information
  7115 Standard Drive
  Hanover, MD 21076–1320

NASA/TM—2007–215189

Modeling of Turbulence Effect on Liquid Jet Atomization

H.P. Trinh
Marshall Space Flight Center, Marshall Space Flight Center, Alabama

National Aeronautics and
Space Administration

Marshall Space Flight Center • MSFC, Alabama 35812

December 2007

Acknowledgments

I wish to express my sincere gratitude to my advisor, C.P. Chen, for his continuous support, guidance, and encouragement throughout the course of this research. My appreciation is also extended to the members of the advisory committee: K. Frendi, G.R. Karr, M.D. Moser, and S.T. Wu. In addition, I would like to thank D.S. Crocker, B. Zuo, and S. Kim for their consultation in the use and modification of the CFD-ACE+ code. My acknowledgment is also extended to CFD Research Corporation, especially to C.E. Smith, for allowing me to utilize their computational fluid dynamic software, computer equipment, and facility in conducting the numerical simulation for this study. My gratitude is also expressed to K.W. Gross for his effort in proofreading the manuscript. I would like to acknowledge NASA Marshall Space Flight Center for offering me a full-time study program, that enabled me to complete my Ph.D. degree. Helpful assistance of librarians at the Redstone Scientific Information Center, Huntsville, AL, in this research is appreciated.

Available from:

NASA Center for AeroSpace Information
7115 Standard Drive
Hanover, MD 21076–1320
301–621–0390

This report is also available in electronic form at
<https://www2.sti.nasa.gov>

TABLE OF CONTENTS

TABLE OF CONTENTS (Continued)

LIST OF FIGURES

LIST OF FIGURES (Continued)

LIST OF TABLES

LIST OF ACRONYMS

CAB	cascade atomization breakup (model)
CFD	computational fluid dynamics
DNS	direct numerical simulation
ETAB	enhanced TAB
KH	Kelvin-Helmholtz (model)
LES	large-eddy simulation
PDF	probability density function
PDPA	phase/doppler particle analyzer
RANS	Reynolds averaged Navier-Stokes
RNG k-ε	renormalized group k-ε turbulence equation model
SMD	Sauter mean diameter
SMR	Sauter mean radius
TAB	Taylor analogy breakup (model)
Tblob	primary breakup model with the inclusion of the turbulence
TM	Technical Memorandum
TTAB	secondary breakup model with the inclusion of the turbulence

NOMENCLATURE

0	initial value; value at initial time step used in the finite difference formulation
–1	value at a time step before initial time step in finite difference formulation
A_1	constant (0.188)
a	radius of blob or parent drop
a_{af}	parameter after mass stripping from blob drop in primary breakup
a_{be}	parameter before mass stripping from blob drop in primary breakup
B_0	constant (0.61)
B_1	constant (10)
b	collision impact parameter
b_{cr}	critical value of collision impact parameter
C_a	constant ($B_0/3.726B_1$)
C_b	constant (1/2)
C_D	drag coefficient of a deformed droplet
C_d	discharge coefficient of injection nozzle; constant (5)
C_F	constant (1/3)
C_E	turbulence constant
C_e	turbulence constant (1.92)
C_{jet}	constant (10)
C_k	constant (8)

NOMENCLATURE (Continued)

C_m	turbulence constant (0.09)
C_p	constant associated with normalized condition of P
C_t	empirical constant involving turbulence motion
C_ε	turbulence constant (1.92)
c_t	weighting parameter associated with turbulence motion
c_w	weighting parameter associated with surface motion
D	diameter of injection nozzle
d	coefficient associated with viscous damping
d_{max}	maximum possible diameter of product drop
d_{min}	minimum possible diameter of product drop
d_t	diameter of the product drop
d	damping force created by liquid viscous effect
E	energy
E_k	kinetic energy
E_{kt}	energy associated with surface wave motion
E_{osc}	oscillation and distortion energy of the parent drop
E_{par}	total energy of the parent drop prior to breakup
E_{prod}	energy after breakup
E_{surf}	minimum surface tension of the parent drop
E_{tur}	turbulent kinetic energy
F	aerodynamic force acting on the drop

NOMENCLATURE (Continued)

F_t	force associated with turbulence motion in a liquid droplet
g	value of ambient gas
i	$\sqrt{-1}$
I_0	zero-order modified Bessel function of the first kind
I_1	first-order modified Bessel function of the first kind
I_1'	first derivative with respect to time
I_2	second-order modified Bessel function of the first kind
I_n	*n*th-order modified Bessel function of the first kind
I_n'	time derivative of *n*th-order modified Bessel function of the first kind
K	constant (10/3)
K_0	zero order of the second kind
K_1	first-order modified Bessel function of the second kind
K_c	loss coefficient due to nozzle inlet geometry
K_n	first-order modified Bessel function of the second kind
K_n'	time derivative of *n*th-order modified Bessel function of the second kind
K_e	turbulence constant
K_ε	proportionality constant
k	wave number used in the primary breakup formulation; coefficient associated with surface tension; turbulent kinetic energy per unit mass in the *k-e* model
k_0	initial turbulent kinetic energy
k_{bt}	turbulent kinetic energy of the parent drop at the breakup time

NOMENCLATURE (Continued)

k_e	coefficient parameter
k_t	turbulent kinetic energy
k_ζ	droplet shape restoring force caused by surface tension
L	length of injection nozzle
L_e	length of turbulence eddy
L_{jet}	liquid jet intact length
L_t	characteristic length scale associated with turbulence
L_w	characteristic length scale associated with surface motion
m	mass of drop
m_{br}	stripped mass of blob drop during primary atomization process
N	number of drops
N_2	number of drops in parcel 2
N_{prod}	number of product drops
n	number of probable collisions; value at present time step used in the finite difference formulation; number of drops to be taken away from parcel
n+1	value at next step in finite difference formulation
n–1	value at previous time step used in the finite difference formulation
P	probability density function
$P(dt)$	probability density function of droplet diameter
p	pressure
p_l	pressure of the liquid

NOMENCLATURE (Continued)

p_g	gas pressure
$P(n)$	Poisson distribution associated with drop
q	random number on the interval (0,1)
$\Re$	real part of a complex function
Re	Reynolds number
Re_l	Reynolds number of the liquid
r	radial coordinate of a cylindrical jet
r_1	drops with a large radius
r_2	drops with a small radius
r_{32}	Sauter mean radius of product drop
r_p	radius of a parent drop used in the secondary breakup formulations; radius of a product drop used in the primary breakup formulations
r_t	radial length scale associated with turbulence motion
r_w	radial length scale associated with surface wave motion
s	contraction area ratio of injection nozzle
T	Taylor parameter
t	time
t^*	characteristic breakup time
t_{bt}	time when the secondary breakup is complete
t_d	term defined in equation as $\left(C_d \mu_l / 2\rho_l r_p^2\right)$
U	liquid jet injection velocity

NOMENCLATURE (Continued)

u	tangential surface velocity component
u'	fluctuation velocity at nozzle exit
u^2	square of the turbulent fluctuation velocity
u_p	parent drop axial velocity
V	blob or parent drop velocity
Vol	volume of a computational cell
V_{prod}	velocity of the parent drops
v	normal surface velocity component; first normal velocity component of a product drop with respect to the path of parent drop
v_l	dynamic viscosity of the liquid; radial liquid velocity component
W	relative drop velocity with respect to local gas velocity
We	Weber number
We_l	Weber number using the liquid density
We_g	Weber number using the gas density
w	second normal velocity component of product drop referenced to the path of parent drop
x	axial coordinate on the liquid injection direction
y	nondimensional parameter of distortion displacement
ΔE	change in energy of parent drop
ΔP	pressure drop of the injection nozzle
ΔP_{acc}	flow acceleration pressure drop
ΔP_{form}	pressure drop associated with the nozzle entrance shape
ΔP_{noz}	pressure drop due to the wall shear stress

NOMENCLATURE (Continued)

ΔP_{tot}	total pressure drop
Δt	incremental step time in finite difference formulation
ε	dissipation rate of turbulent kinetic energy per unit mass
ε_0	initial dissipation rate
ε_{bt}	dissipation rate of the parent drop at the breakup time
ε_t	dissipation rate of turbulent kinetic energy
ζ	radial cross-section change from its equilibrium position (displacement of the equator of the droplet from its equilibrium position)
Z	Ohnesorge number
η	surface perturbation displacement
η_0	infinitesimal amplitude
λ	surface wavelength
Λ	wavelength of fastest growing wave
μ	viscosity
μ_l	liquid viscosity
ν	dynamic viscosity
ν_{12}	collision frequency of droplets contained in any parcel pairs
ρ	density
ρ_l	liquid density
ρ_g	gas density
σ	surface tension coefficient
τ	time associated with surface wave motion

NOMENCLATURE (Continued)

τ_t	characteristic time scale associated with turbulence
τ_w	characteristic time scale associated with surface wave motion
υ	collision frequency
ϕ	angle randomly generated on the interval
$\Phi(dt)$	turbulence energy spectrum associated with droplet diameter dt
ω	wave growth rate used in the primary breakup formulations; angular frequency used in the secondary breakup formulations
Ω	maximum wave growth rate
.	first derivative with respect to time
..	secondary derivative with respect to time
$\mathfrak{I}$	wave number

TECHNICAL MEMORANDUM

MODELING OF TURBULENCE EFFECT ON LIQUID JET ATOMIZATION

1. INTRODUCTION

Recent experimental investigations and physical modeling studies have indicated that turbulence behaviors within a liquid jet have considerable effects on the atomization process. Such turbulent flow phenomena are encountered in most practical applications of common liquid spray devices. Most of the existing atomization models do not account for turbulence effects. Limited attempts have been made to model the subject effects on liquid jet disintegration; however, they treat turbulence as either an only source or as a primary driver in the breakup process.

This research aims to model the effects of turbulence occurring inside a cylindrical liquid jet to its atomization process. Although considerable research has been oriented to liquid atomization processes for more than a century by many authors, only work that is closely relevant to this investigation is considered and presented here. In summary, this research effort contributes to the improvement of predictions in liquid jet atomization processes.

Outlines of the proposed research topic will be presented in the following subsections. The motivation and objective of this research effort are stated along with a discussion of the approach to be taken.

1.1 Background

The transformation of a liquid body into droplet sprays in a gaseous surrounding is of great importance in many industrial processes. Various spray devices have been developed that are designated as atomizers or injectors. In liquid fuel combustion systems, such as rocket engines, diesel engines, gas turbines, and industrial furnaces, the combustion efficiency and chemical reaction behavior are primarily dependent on the effectiveness of the liquid body broken up into sprays. Smaller drop sizes, generated from the spray devices, increase the specific surface area of the fuel and thereby achieve high rates of evaporation and mixing. Consequently, higher engine efficiency would be realized in the combustion process. On the other hand, mixed fuel that reacts rapidly near the injector could cause the injector exit surface to inadvertently overheat. These phenomena have been observed in many liquid rocket engines during their hardware development phase. Therefore, understanding and adequately predicting this physical breakup process leads to designing better spray devices for these various applications.

In general, the transformation of a liquid jet into droplet sprays can be divided into two separate stages as portrayed in figure 1. Lefebvre describes the mechanisms of the jet breakup as follows: “When a liquid jet emerges from a nozzle as a continuous body of cylindrical form, the competition set up on

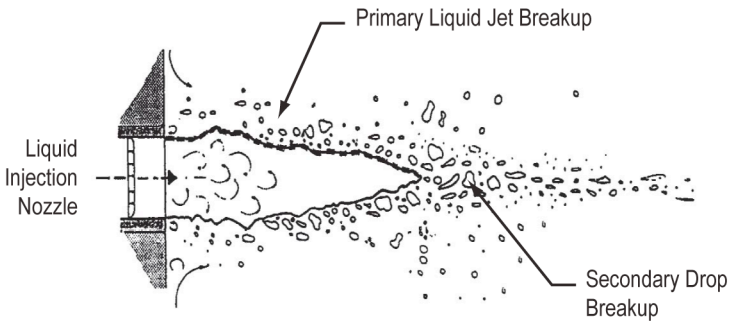

Figure 1. Sketch of primary and secondary liquid jet breakup regimes.

the surface of the jet between the cohesive and disruptive forces gives rise to oscillations and perturbations. Under favorable conditions the oscillations are amplified and the liquid body disintegrates into drops."[1] This process is sometimes referred to as primary atomization or primary liquid jet breakup. Moving downstream, the liquid further breaks up into smaller drops. This process is also known as secondary atomization (secondary droplet breakup).

The mechanisms of atomizing the liquid jet are complex. Jet inertial and aerodynamic forces along with the surface tension certainly play a role in the breakup process. In addition, interaction of the liquid with turbulent gas flow also contributes to the jet disintegration. Considerable studies have been dedicated to gain knowledge and subsequently model this phenomenon. Faeth and Crowe et al. provide substantial reviews on this topic.[2,3]

Many researchers have also reported that for certain favorable flow conditions turbulent motion can be recognized within the liquid jet. Often the geometrical sharpness of the injection nozzle inlet, along with appropriate flow conditions, can create cavitations inside the nozzle. The collapse of this cavitation can generate a flow fluctuation, leading to a more aggressive disintegration of the liquid jet. The turbulent primary breakup was first reported in 1932 based on visualization studies conducted by De Juhasz et al.[4] In the following years, Schweitzer observed that the level of the liquid turbulence had some effect on the jet stability.[5] Later investigations of the turbulent liquid jet breakup in quiescent air were performed by various authors, including Chen and Davis, Grant and Middleman, Phinney, and McCarthy and Mallory.[6–9] They observed that disintegration of the liquid jet occurred rapidly near the nozzle exit in certain flow regimes. Using the measured data, Grant and Middleman were able to correlate the flow conditions and liquid breakup lengths. Phinney conducted a series of experiments in which the liquid jets were propelled into a gaseous atmosphere from injection tubes at various fluid conditions ranging from laminar to fully developed turbulent flows. Similar to Grant and Middleman, Phinney also came up with a correlation of breakup lengths based on dimensional analyses. His results showed that the breakup length of the liquid core was significantly shortened when the liquid jet changed from laminar to turbulent flow. The author also observed the appearance of fine milk-white droplet clouds at the injection ports.

With the advancements of nonintrusive measurement techniques, introduced in the 1980s, researchers have been able to experimentally discover more physical details and provide more measured data for subject atomization. Studies of relatively large-size liquid jets, performed by Wu et al. and

Tseng et al., provided droplet data, such as size, velocity, and fluctuation quantities, and reported a more complete mechanistic approach for the primary atomization regime.[10–14] During the investigation of fully developed turbulent round jet sprays, Wu et al. and Tseng et al., observed that when turbulence developed inside the jet column, starting at the nozzle exit, this turbulence motion remained dominant and became a main contributor in the spray development. The authors believed that this turbulence characteristic played a primary role on the liquid stripping near the injector exit. Tseng et al. also indicated that drop sizes after the primary breakup, in general, were larger for turbulent than nonturbulent liquids. Based on the data collected from their experiments, the authors were able to establish correlations between the turbulence fluctuation quantities, the breakup drop size, and the breakup length of the liquid jet. Further studies of turbulent liquid jets flowing into a quiescent gas were also performed by Sallam et al.[15,16] They characterized the liquid breakup by a series of flow visualizations as well as phenomenological analysis. The results showed that the breakup regimes for the turbulent liquid jets can be described in a way similar to the existing theories of nonturbulent liquid jets, and these regimes can be fully expressed by the turbulence flow properties.

1.2 Previous Research on Atomization Modeling

In the arena of atomization modeling, various theories and models for cylindrical jet atomization have been proposed. In 1879, Rayleigh studied the linear stability of an infinitely long, circular, inviscid, incompressible liquid jet.[17] He was able to derive an expression for the growth of surface disturbances as a function of time. This theory works reasonably well for the low-Weber number regime. Theoretical work and model development, based on the Kelvin-Helmholtz (KH) instability of the liquid surface wave, has continued to grow significantly over the years. Comprehensive reviews on this classical work can be found in McCarthy and Bogy.[9,18] Later, Rangel and Siringnano, and Clark and Dombrowski extended the surface instability theory for the liquid jet and sheet breakup to include higher order terms that account for the effects of surface tension and liquid-to-gas density ratio.[19–21]

For the last few decades, developments and enhancements of ink-jet printing, diesel fuel injection, and direct injection techniques in automobile engines and liquid rocket engines have required further improvements of liquid injection predictions. In addition, improved computational techniques and advanced computer capabilities have promoted further research in this modeling arena. As to the convenience of implementing improvements to computational fluid dynamic (CFD) methods and the wide utilization by analysts, the two most noticeable atomization models are the KH instability of Reitz and the Taylor analogy breakup (TAB) model of O'Rourke and Amsden.[22,23] Reitz derived the KH model, also known as the blob model or stripping rate model, which described the primary breakup entirely in terms of the surface wave perturbation, in which viscosity, surface tension, and aerodynamic forces were the contributing factors. On the other hand, the TAB model was based on an analogy between an oscillating distorting droplet and a spring-mass system. In this model the drop distortion was driven by the force interaction between the external aerodynamic surface tension and the viscous damping of the droplet liquid. The TAB model is suitable for predicting the secondary breakup regime. Further reviews of these two models can be found in section 2. Recently, Tanner examined data from liquid jet breakup experiments at high-pressure conditions and found that an intact liquid core is broken into various liquid shapes or drop sizes shortly after the injection exit port.[24] Hence, the author extended the TAB model and developed an enhanced TAB (ETAB) model to include the primary breakup regime. Tanner also accounted for the droplet surface stripping near the injector exit with a power law drop-size distribution using his recent cascade atomization breakup (CAB) model for high-pressure liquid jets.[25]

Though these models in some aspects provide reasonable predictions of the liquid atomization, they do not account for the liquid turbulence motion observed in certain sprays as previously described. In a study of primary diesel fuel atomization, Nishimura and Assanis developed a phenomenological cavitation model in which the primary breakup is governed by the turbulence mechanism.[26] Turbulence energy is formed by bubble collapse and fluid turbulence motion. To consider the nozzle exit turbulence conditions of diesel spray modeling in the atomization process, Huh et al. proposed a scheme taking into account two independent mechanisms—wave growth and turbulence.[27] The turbulence is characterized partially by the injection nozzle geometry, while the wave growth is derived from the KH instability theory. A logical framework of coupling the flow inside the injection nozzle to the jet breakup can be achieved with this approach. The rationale for this approach is based on an order of magnitude analysis of the flow dynamic breakup mechanisms and those associated with the turbulence. This analysis concludes that gas inertia force and turbulent stress are the two main forces in the atomization of typical diesel engine injectors. In this model, the breakup rate for the parent drops is set to be proportional to the length scale-to-time scale ratio. It is hypothesized that the turbulence length scale is more dominant in the primary breakup while the wavelength scale is more important for the secondary droplet breakup. On the other hand, the time scale is a linear sum of the turbulence and wave growth time scales.

The aforementioned models were formulated with semiempiricism. The associated coefficients had to be determined with reference to experimental data. Another class of atomization models was derived based on the conservation laws of mass, momentum, and energy. By taking advantage of improvements in CFD techniques, as well as new computer capabilities, the hydrodynamic equations that account for nonlinear effects can be directly solved. Various numerical computations using the volume-of-fluid method, as proposed by Fromm, Child and Mansour, Shokoohi and Elrol, and more recently Liang and Ungewitter, represent the first attempts of direct simulation without using the wave instability theories.[28–31] In their analyses, the Navier-Stokes equation system has been numerically solved to predict the interfacial instability and jet breakup. Their results generally agree with the measured data for low-velocity injection conditions. Yang et al. proposed to solve the jet hydrodynamic equations which also accounted for the nonlinear inertia terms and full nonlinear capillary pressure terms.[32]

Several efforts using more sophisticated numerical approaches have been performed recently modeling the detailed turbulent flow fields in liquid and gas during the atomization process. Klein And Janicka and De Villiers et al. computed the two-phase flows using the large eddy simulation (LES) method.[33,34] For the first time, De Villiers et al. were able to apply a numerical technique to resolve jet atomization under the more realistic operating conditions found in diesel engines. Leboissetier and Zaleoki also attempted to simulate a liquid spray with a multidimensional pseudo direct numerical simulation (DNS) method.[35]

The aforementioned numerical methods have a real potential of providing a complete physical description of the liquid jet breakup with minimum assumptions; however, they require small computational time steps and fine grids across the entire jet domain for their simulations. The LES and DNS techniques, in particular, may need submicron spatial elements in size and pico-second in time steps to properly predict the atomizing sprays at the high-velocity injection conditions. Consequently, grid mesh size and the considered physical domain must be taken care of so that the computational time and memory storage requirements will be manageable. At the present time these techniques are still too expensive and generally impractical in terms of computational time and power requirements for

engineering calculation applications. Hence, engineering analysis and design of the liquid spray devices must still rely on physical engineering models.

1.3 Motivation and Objective

The previous reviews demonstrate that researchers have observed the natural existence of turbulence within liquid jets for certain flow conditions. Generally, this flow fluctuation can be formed by favorable flow conditions, for instance, a fully developed turbulent flow in a long cylindrical tube. Sometimes it can also be created from the collapse of cavitation bubbles inside the injection nozzle. The cavitation is induced by the shape of the nozzle, such as a sharp nozzle entrance or nozzle curvature. Unfortunately, the aforementioned turbulent flow conditions are present in most applications of common liquid spray devices. Moreover, results of past experiments suggest that turbulence motion within the liquid may alter the intact jet core, as well as the production of drops that have a different size in comparison to the droplet breakup without the turbulence consideration. Undoubtedly, an accurate modeling of such turbulence effects on the atomization process would significantly enhance the prediction capability of existing physical models. Limited attempts have been made in modeling the turbulence phenomenon on liquid jet disintegration. Nonetheless, subject correlation and models treat the turbulence either as an only source or as a primary driver in the breakup process. Other computations of the liquid atomization have been performed using DNS; however, these sophisticated numerical simulations are computationally unaffordable at the present time.

Hence, the present research aims to model the turbulence effects on the primary and secondary atomization processes. Such models can be implemented in numerical simulations to predict the breakup process of a cylindrical liquid jet. This proposed effort enhances the existing atomization models so they can predict the liquid breakup with more physically realistic conditions.

1.4 Research Approach

In the course of this study, terms accounting for the turbulence motion within a liquid were developed based on a phenomenological point of view. These terms are appropriately supplemented to the two classical atomization models—KH primary breakup of Reitz and TAB secondary breakup of O'Rourke and Amsden.[22,23] In the primary atomization model, the level of turbulence effects, on the mass stripping of blob drops and product drop sizes are represented by the characteristic time and length scales and kinetic energy. This treatment offers contributions of individual physical phenomena on the liquid breakup. For the secondary breakup, an additional turbulence effect, acted on the parent drops, is modeled and integrated into the TAB governing equation. This turbulence term is referenced to the dissipation rate of the turbulent kinetic energy and the deformation rate of the parent drop distortion displacement. All associated empirical constants used in these additional terms are determined by matching the results with available measurements. Two computer programs have been written to simulate these proposed models. Results of the new and existing models are compared and fully appraised. Finally, these models are implemented into existing CFD simulations. The predicted results are evaluated with the available experimental data.

2. REVIEW OF EXISTING ATOMIZATION MODELS OF LIQUID JETS

This section provides an extensive review of the KH instability model of Reitz and the TAB model of O'Rourke and Amsden, since the proposed models are based on these two methods.[22,23] The material in this section provides complete descriptions and formulations of the two subject models. The governing equations of the liquid surface wave motion are reviewed leading to the blob primary jet breakup model. Expressions for the mass stripped from the blob drop and the produced drop size are also presented. The TAB model derivation is reviewed, concentrating on the forces acting on a liquid droplet immersed in a gaseous flow field. The equation for estimating the product drop size is also formulated. As stated earlier, the KH instability and TAB for primary and secondary atomization are the basic foundation for formulating the turbulence terms included in these models.

2.1 Kelvin-Helmholtz Instability: Primary Atomization Model

The original formulation of this primary breakup model was based on the stability analysis performed by Reitz and Bracco.[36] They examined the surface stability of a cylindrical liquid jet that is subject to perturbations using a first-order linear theory. The surface perturbation and consequential drop breakup can be visualized by the sketch shown in figure 2. This sketch shows a blob of liquid with surface waves at its interface. The waves continue to grow in amplitude until the breakup occurs and then the product drops are formed. The analysis starts by imposing an infinitesimal axisymmetric perturbation displacement of the form on the surface:

$$\eta = \Re\left(\eta_0 e^{ikx+\omega t}\right) , \tag{1}$$

where

$$i=\sqrt{-1} .$$

The displacement (η) is a real part ($\Re$) of a function, which contains variables of the time (t) and the axial distance (x) in reference to the initial jet injection time and respective nozzle exit location. η is related to the growth rate (ω) of an initial perturbation of infinitesimal amplitude (η_0) to its wave number (k).

By applying the linearized hydrodynamical equations for the liquid and gas, the inviscid gas equations of motion yield for the gas pressure at the interface $r=a$

$$p_g = -\rho_g\left(W - i\frac{\omega}{k}\right)^2 k\eta\frac{K_0(ka)}{K_1(ka)} , \tag{2}$$

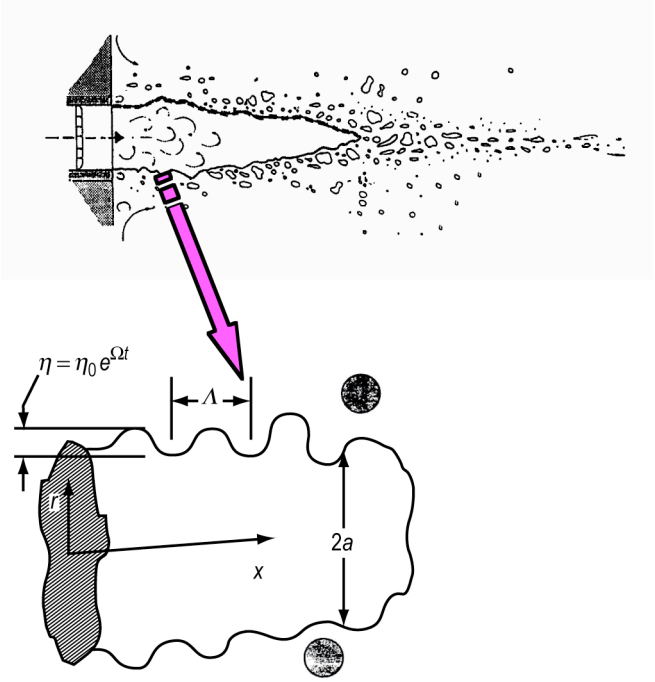

Figure 2. Schematic showing surface waves and breakup of a liquid blob.

where r is the radial coordinate of the cylindrical liquid jet, while p_g and ρ_g are the gas pressure and density, respectively. W is the magnitude of the relative velocity between the liquid and gas. K_0 and K_1 are zero and first-order modified Bessel functions of the second kind. With the assumption that $\eta << a$, the kinematic, tangential stress, and normal stress equations at the interface can be expressed as

$$v_l = \frac{\partial \eta}{\partial t} \quad , \quad \frac{\partial u_l}{\partial r} = -\frac{\partial v_l}{\partial x} \tag{3}$$

and

$$-p_l + 2\upsilon_l \rho_l \frac{\partial v_l}{\partial r} - \frac{\sigma}{a^2}\left(\eta + a^2 \frac{\partial^2 \eta}{\partial x^2}\right) + p_g = 0 \quad . \tag{4}$$

The axial and radial liquid velocity components u_l and v_l are along the liquid surface. Surface tension, dynamic viscosity, density, and pressure of the liquid are σ, υ_l, ρ_l, and p_l, respectively. Solving equation (4) along with the substitutions of equations (1)–(3) results in a dispersion relationship as follows:

$$\omega^2 + 2\upsilon_l k^2 \omega \left[\frac{I_1'(ka)}{I_0(ka)} - \frac{2k\Im}{k^2 + \Im^2} \frac{I_1(ka)}{I_0(ka)} \frac{I_1'(\Im a)}{I_1(\Im a)} \right]$$

$$= \frac{\sigma k}{\rho_l a^2} \left(1 - k^2 a^2\right) \left(\frac{\Im^2 - k^2}{\Im^2 + k^2} \right) \frac{I_1(ka)}{I_0(ka)}$$

$$+ \frac{\rho_g}{\rho_1} \left(W - i\omega/k\right)^2 k^2 \left(\frac{\Im^2 - k^2}{\Im^2 + k^2} \right) \frac{I_1(ka)}{I_0(ka)} \frac{K_1(ka)}{K_0(ka)} \ , \tag{5}$$

where

$$\Im = \sqrt{k^2 + \omega/\upsilon_l} \ .$$

The above equation contains I_0 and I_1 as the zero and first-order modified Bessel functions of the first kind. The first derivative with respect to time for I_1 is I_1'. Reitz numerically solved equation (5).[22] The results indicate that there is a single maximum in the wave growth rate curve $\omega = \omega(k)$. He further generated curve fits of the numerical solutions to equation (5) for the maximum growth rate ($\omega = \Omega$) and for the corresponding wavelength ($\lambda = \Lambda$) that led to the correlation as follows:

$$\frac{\Lambda}{a} = 9.02 \frac{\left(1 + 0.45Z^{0.5}\right)\left(1 + 0.4T^{0.7}\right)}{\left(1 + 0.87We_g^{1.67}\right)^{0.6}} \tag{6}$$

and

$$\Omega \left[\frac{\rho_l a^3}{\sigma} \right]^{0.5} = \frac{\left(0.34 + 0.38We_g^{1.5}\right)}{\left(1 + Z\right)\left(1 + 1.4T^{0.6}\right)} \ , \tag{7}$$

where

Z = Ohnesorge number $\left(Z = We_l^{0.5} / Re_l\right)$

Re_l = Reynolds number of the liquid $\left(Re_l = Wa/\nu_l\right)$

We_l = Weber number using the liquid density $\left(We_l = \rho_l W^2 a/\sigma\right)$

We_g = Weber number using the gas density $\left(We_g = \rho_g W^2 a/\sigma\right)$

T = Taylor parameter $\left(ZWe_g^{0.5}\right)$.

To implement equations (6) and (7) in the primary atomization prediction, Reitz assumed that the liquid was injected in a monodispersed fashion, of which the liquid jet initially was in a form of blob parcels, containing liquid spherical drops with their size equal to the injection nozzle diameter. Hence, the Reitz model was also interchangeably called the blob model.

Traveling downstream from the injector, the blob drop (also referred to as the parent drop) undergoes surface breakup into product drops (also denoted as children drops) due to a tripping action. This is due to the unstable surface wave driven primarily by the fastest wave growth rate and the corresponding wavelength. The rate of change in the parent drop size is governed by a ratio of the characteristic length and time scales associated with the wave perturbation motion as

$$\frac{da}{dt} = -\frac{a - r_w}{\tau}, \text{ when } r_w \ll a \ . \tag{8}$$

The time (τ) is associated with the surface wave motion while r_w is the radius of the product droplets that are formed from the shredded mass of the parent drop. The parameters r_w and τ are related to the fastest wave growth rate and the corresponding wavelength as

$$r_w = \begin{cases} B_0 \Lambda & (B_0 \Lambda \le a) \\ \min\left[\left(3\pi a^2 W / 2\Omega\right)^{0.33}, \left(3a^2 \Lambda / 4\right)^{0.33}\right] & \left(B_0 \Lambda > a\right) \end{cases} \tag{9}$$

and

$$\tau = 3.726 B_1 a / \Lambda\Omega \ , \tag{10}$$

where the values of B_0 and B_1 are set equal to 0.61 and 10, respectively. The approach used in this study is directed to extend this formulation by including a turbulence term, as shown in the next section. For that reason, it is helpful to rewrite equation (8) as follows:

$$\frac{da}{dt} = -\left[\frac{a}{\tau} - C_a \frac{L_w}{\tau_w}\right], \text{ when } B_0 \Lambda \ll a \ . \tag{11}$$

$L_w = \Lambda$ and $\tau_w = a / \Lambda\Omega$ can be considered as the characteristic length and time scales associated with the unstable surface wave behavior. The coefficient C_a becomes

$$C_a = \frac{B_0}{3.726 B_1} \ .$$

In summary, the blob model that is used to describe the primary breakup was formulated entirely in terms of the surface wave perturbation in which viscosity, surface tension, and aerodynamic forces were the contributing factors. Hence, the present form of this model needs to be modified when turbulence appears in the liquid jet. The proposed enhancement will be discussed in section 3.

2.2 Taylor Analogy Breakup: Secondary Atomization Model

O'Rourke and Amsden constructed the TAB model based on an analogy between an oscillating, distorting droplet and a spring-mass system. Formulation of the subject models is presented in the remainder of this section.

2.2.1 Modeling Droplet Surface Wave Motion

In the TAB model, due to the surface tension and viscous damping of the liquid droplet, drop distortion is driven by external aerodynamic droplet gas interaction force and droplet shape restoring force. The analogy between the droplet distortion and a spring-mass system is shown in figure 3.

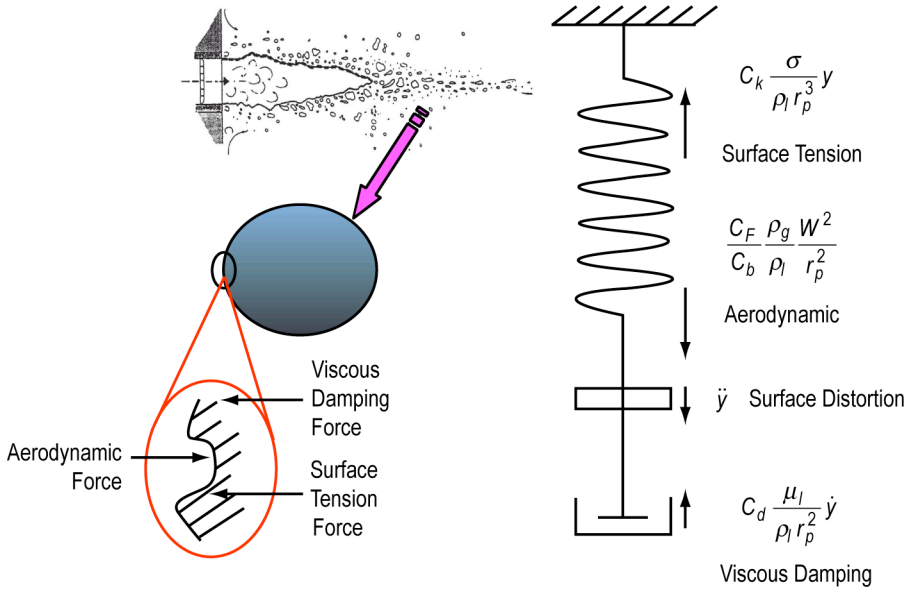

Figure 3. Schematic showing analogy of forces acting on a liquid drop and spring-mass system.

The linear differential equation for a forced dampened harmonic oscillator is written as

$$m\ddot{\xi} = F - k\xi - d\dot{\xi} \quad , \tag{12}$$

where

m = mass of drop
ξ = radial cross-section change from its equilibrium position (displacement of the equator of the droplet from its equilibrium position)
F = force acting on the drop due to the aerodynamic droplet-gas interaction
$k\xi$ = droplet shape restoring force caused by the surface tension
$d\dot{\xi}$ = damping force created by the liquid viscous effect.

Formulations for the coefficients used in the terms of equation (12) are

$$\frac{F}{m} = C_F \frac{\rho_g W^2}{\rho_l r_p}$$

$$\frac{k}{m} = C_k \frac{\sigma}{\rho_l r_p^3}$$

$$\frac{d}{m} = C_d \frac{\mu_l}{\rho_l r_p^2} \ ,$$

where ρ_g and ρ_l are the gas and liquid densities, W is the relative velocity between the local gas and the droplet, r_p is the droplet radius, σ is the liquid surface tension coefficient, and μ_l is the liquid viscosity. Based on matching the analytical results with experimental data the constants C_F, C_k, and C_d are set to 1/3, 8, and 5, respectively.

To nondimensionalize the distortion displacement (ζ), y is set equal to $\zeta / C_b r_p$, where C_b is a constant. When substituting this nondimensional parameter and the coefficient formulations into equation (12), it can be rearranged as

$$\ddot{y} = \frac{C_F}{C_b} \frac{\rho_g}{\rho_l} \frac{W^2}{r_p^2} - C_k \frac{\sigma}{\rho_l r_p^3} y - C_d \frac{\mu_l}{\rho_l r_p^2} \dot{y} \ . \tag{13}$$

Equation (13) is a linear, nonhomogeneous second-order differential equation. It has an exact solution as

$$y(t) = \frac{C_F}{C_k C_b} We + e^{-t/t_d} \left[\left(y_0 - \frac{C_F}{C_k C_b} We \right) \cos \omega t + \frac{1}{\omega} \left(\dot{y}_0 + \frac{y_0 - \frac{C_F}{C_k C_b} We}{t_d} \right) \sin \omega t \right] \ , \tag{14}$$

where

$$We = \frac{\rho_g W^2 r_p}{\sigma}$$

$$\frac{1}{t_d} = \frac{C_d}{2}\frac{\mu_1}{\rho_l r_p^2}$$

$$\omega^2 = C_k \frac{\sigma}{\rho_l r_p^3} - \frac{1}{t_d^2} \quad .$$

The Weber number and angular frequency of the oscillatory motion are denoted as We and ω. The values of y and its first derivative at $t = 0$ are y_0 and $\dot{y}_0$.

2.2.2 Drop-Size Estimation From TAB Model

The Sauter-mean radius (SMR) of the product drops is derived from the energy balance before and after droplet breakup. Prior to the breakup, the energy of the parent drop is represented by the minimum surface tension energy (E_{surf}) and the oscillation and distortion energy (E_{osc}) that are defined as follows:

$$E_{surf} = 4\pi r_p^2 \sigma \tag{15}$$

$$E_{osc} = K\frac{4\pi}{5}\rho_l r_p^3\left(\dot{\xi}^2 + \omega^2\xi^2\right) = K\frac{\pi}{5}\rho_l r_p^5\left(\dot{y}^2 + \omega^2 y^2\right) \quad . \tag{16}$$

The constant (K) is the ratio of the total energy from distortion and oscillation to the energy in the fundamental model. The value of $K=10/3$ has been obtained by matching analysis data with experiment data. So, the total energy of the parent drop prior to the breakup (E_{par}) is

$$E_{par} = E_{surf} + E_{osc} = 4\pi r_p^2\sigma + K\frac{\pi}{5}\rho_l r_p^5\left(\dot{y}^2 + \omega^2 y^2\right) \quad . \tag{17}$$

It is assumed that the product drops are not distorted or oscillating after breakup. Thus, the energy after breakup (E_{prod}) would only contain the minimum surface energy and the kinetic energy of the motion normal to their parent droplet

$$E_{prod} = 4\pi r_p^2\sigma\frac{r_p}{r_{32}} + \frac{\pi}{6}r_p^5\rho_l\dot{y}^2 \quad . \tag{18}$$

By equating equations (17) and (18) the SMR (r_{32}) of the product drops, formed after the secondary atomization, can now be calculated as

$$E_{prod} = E_{par}$$

$$r_{32} = \frac{4\pi r_p^3 \sigma}{E_{par} - \frac{\pi}{6} r_p^5 \rho_l \dot{y}^2} \quad . \tag{19}$$

As mentioned in section 1, the liquid turbulence phenomenon has been encountered in certain spray conditions. Earlier investigations of such turbulence characteristics suggest that these turbulence behaviors also contribute to the jet breakup process.[8,10,13–16] Fluctuation of the liquid properties can be generated from the turbulent flow conditions that exist inside the injection nozzle. In addition, injection nozzle hardware geometry and surface roughness can increase the fluctuation; however, the present analytical formulations of these models are not able to capture this physical behavior. This research is focused to model the liquid turbulence effects and incorporate them into existing breakup models, with the goal of improving the breakup process prediction in a more realistic fashion. Modifications of the KH and TAB models are proposed in section 3.

3. MODELING OF TURBULENCE EFFECT ON LIQUID JET BREAKUP

This section presents the derivation of the primary atomization model (Tblob) for the turbulent liquid jet. All physical models and closure expressions associated with this breakup regime are shown. This section focuses on formulation of the terms to account for the turbulence effect on the primary atomization. These terms are derived based on the phenomenological approach. The expression representing the rate of change in the blob drop size is modified and the turbulence characteristic scales to be used in the primary breakup model are formulated. The proposed estimation of the product drop size and its velocity are also presented. Finally, the expression for estimating the initial turbulence quantities of the product drop is developed.

3.1 Rate of Change in Parent Drop Size

The main contribution of this research effort is oriented to incorporate the turbulence effect in modeling of the liquid jet breakup. As mentioned in section 2, the blob model is extended to include terms and parameters associated with the turbulence behavior. Hence, it may be proper to designate the present model as the Tblob model. The phenomenological approach is chosen in this model development to account for both the effects of surface wave perturbation and turbulence motion. The resulting model should adequately include the combination of these two phenomena when both coexist in the considered flow conditions; however, the model is also capable of describing the breakup caused by surface wave perturbation when the turbulence is not present in certain flow conditions. In such a case, the original formulation should be retained. For all aspects, the model should reasonably maintain a smooth transition from the nonturbulent to fully turbulent flow regimes. Also in this phenomenological method, the kinetic energies associated with surface wave and turbulence motions are used to weight these individual effects. Consideration of the kinetic energy level for this weighting is based on the phenomenon that the larger kinetic energy motion would have a stronger influence in the liquid jet breakup process.

In the proposed primary breakup model, length and time scales are composed of those described in the KH model, representing surface wave instability and turbulence behavior. Subject turbulence is characterized using the framework developed by Huh et al.[27]

To derive the new model, it is proposed that the rate of change in the parent drop radius has a similar formulation as shown in the Reitz model, equation (11), with an inclusion of the turbulence term

$$\frac{da}{dt} = -\left[\frac{a}{\tau} - C_a\left(\frac{L_w}{\tau_w} - \frac{L_t}{\tau_t}\right)\right], \text{ when } r_p \ll a \quad . \tag{20}$$

L_t and τ_t are the turbulence characteristic length and time scales, respectively, and r_p is the radius of the product drop. These parameters will be defined later in this section. The third term on the right-hand side of equation (20) represents the contribution of the turbulence effect on the stripping rate of the

parent drop. This turbulence term would accelerate the reduction in the parent drop radius with time. As expected, the primary breakup should be complete earlier than for the case without the turbulence. This result is consistent with the experimental observations of Phinney, Soteriou et al., Chaves et al., and Schimdt et al. in which the liquid jet has a short intact core length when turbulence appears due to the flow at a high Reynolds number or cavitation.[8,37–39] The contribution of the unstable surface wave to the primary breakup is reflected in the first and second terms on the right-hand side of the equation. They are the same terms as shown in the Reitz model. It should be noted that the third term would vanish when turbulence does not exist in the fluid. In such a case, equation (20) would become the original blob model of Reitz that only retains the effect of the surface wave motion on the primary breakup.

Similar to the criterion set by Reitz, the parent drop would no longer strip its mass to create the product drop when $a \le r_p$. Instead, the radius of the subject drop would be adjusted with equation (25), derived in the next section; therefore, equation (20) is of no use for such a situation.

3.2 Turbulence Characteristic Length and Time Scales

In the work of Huh et al., the parent drops were assumed to carry homogeneous isotropic turbulence starting at the injection nozzle exit.[27] Assuming further that no additional internal turbulence is generated, the authors were able to obtain an analytical solution of the turbulence scale through the use of the well-known k-ε turbulence model. Details of this derivation can be found in appendix A. The turbulence time scale can be expressed as a function of time as

$$\tau_t = \tau_t^0 + 0.0828t \ . \tag{21}$$

The time (t) is counted from the time that the parent drop leaves the injection nozzle exit. The initial turbulence time scale (τ_t^0) is evaluated from the initial turbulent kinetic energy (k_t^0) and its corresponding dissipation rate (ε_t^0) at the injector exit:

$$\tau_t^0 = C_\mu \frac{k_t^0}{\varepsilon_t^0} \ , \tag{22}$$

where

$$C_\mu = 0.09$$

$$k_t^0 = \frac{U^2}{8\,L/D}\left[\frac{1}{C_d^2} - K_c - \left(1 - s^2\right)\right]$$

$$\varepsilon_t^0 = K_\varepsilon \frac{U^3}{2L}\left[\frac{1}{C_d^2} - K_c - \left(1 - s^2\right)\right]$$

$$K_\varepsilon = 0.27 \ .$$

The velocity (U) is a liquid velocity at the injection nozzle that has the length (L) and the diameter (D). The discharge coefficient, the loss coefficient due to the sharpness of the nozzle entrance, and the downstream-to-upstream contraction area ratio of the injection nozzle are represented by C_d, K_c, and s, respectively. Formulations of k_t^0 and ε_t^0 are derived in appendix A.

The turbulence characteristic length scale (L_t) can be derived in the same way as τ_t. Huh et al. formulated L_t as a function of the time and the initial turbulence scales by using the analytical solution of the k-ε turbulence model:

$$L_t = L_t^0 \left(1 + \frac{0.0828t}{\tau_t^0} \right)^{0.457} . \tag{23}$$

Similarly to evaluating τ_t^0, the initial turbulence length scale (L_t^0) is obtained from the turbulent kinetic energy and its dissipation rate as

$$L_t^0 = C_\mu \frac{\left(k_t^0\right)^{3/2}}{\varepsilon_t^0} . \tag{24}$$

Again, details of derivations for the turbulence length scale can be found in appendix A.

3.3 Product Drop Size and Velocity

Results from studies of turbulent liquid jets, performed by Tseng et al., show that drops produced from the onset breakup regime have sizes in the same order of magnitude of the turbulence length scale. On the other hand, with consideration of the surface wave perturbation, Reitz set the product drop radius, shown in equation (9), to be proportional to the wavelength associated with the fastest growth rate. The above relations suggest that it is reasonable to formulate the radius of the product drops with the characteristic length scales for both the wave perturbation and turbulence phenomenon.

For the present model, the reciprocal of the product drop radius is expressed by the sum of the reciprocals of the length scales associated with surface wave instability and turbulence motion, with the inclusion of the respective weighting factors as follows:

$$\frac{1}{r_p} = \frac{c_w}{r_w} + \frac{c_t}{r_t} \Rightarrow r_p = \frac{r_w r_t}{\left(1 - c_t\right) r_t + c_t r_w} . \tag{25}$$

The radius of the product drop is r_p. The radius (r_w) associated with the wave motion can be determined from the Reitz model, as shown in equation (9). The weighting coefficients (c_w) and (c_t) are determined by the kinetic energy ratio of the turbulence motion and wave perturbation. These are defined later in this section.

The value of r_t is estimated from the formulations proposed by Huh et al. The authors hypothesized that the drop size could be represented by a probability density function (PDF) proportional to the ratio of the turbulence energy spectrum and the atomization time scale. The notion for this representation was that an eddy motion with larger turbulent kinetic energy and a shorter atomization time most likely caused the drop breakup to occur more frequently than those containing the lower energy level and the longer atomization time. By assigning the wave number of the turbulence energy spectrum as the inverse of the product drop diameter, it can be shown that

$$r_t = \frac{1}{2} \frac{\int_{d_{min}}^{d_{max}} \frac{x\left(k_e x\right)^{-2}}{\left[1+\left(k_e x\right)^{-2}\right]^{11/6}} dx}{\int_{d_{min}}^{d_{max}} \frac{\left(k_e x\right)^{-2}}{\left[1+\left(k_e x\right)^{-2}\right]^{11/6}} dx} \quad , \tag{26}$$

where

k_e = $0.75/L_t$
d_{max} = Maximum possible diameter of the product drop
d_{min} = Smallest possible diameter of the product drop.

The detailed derivation of the equation above can be found in appendix A. The weighting coefficient (c_t) used in equation (25) is simply formulated with the kinetic energy terms related to the surface wave and flow turbulence levels as

$$c_t = \frac{E_{kt}}{E_{kt} + E_{kw}} \quad , \tag{27}$$

where

$$E_{kt} = \left(\frac{L_t}{\tau_t}\right)^2$$

$$E_{kw} = \left(\frac{L_w}{\tau_w}\right)^2 = \left(\frac{\Lambda^2 \Omega}{a}\right)^2 \text{ with } L_w = \Lambda \text{ and } \tau_w = a/\Lambda\Omega \quad .$$

The relation of c_t and the kinetic energy ratio E_{kt}/E_{kw} is graphically displayed in figure 4. The expression of c_t, as shown in equation (27), is obeyed to three constraints: (1) When $E_{kt} \ll E_{kw}$, c_t approaches zero; (2) when $E_{kt} \gg E_{kw}$, c_t becomes 1; and (3) if $E_{kt} = E_{kw}$, c_t is set equal to 0.5. These constraints impose a balanced contribution of the wave perturbation and turbulence effect on the liquid jet breakup and also provide a smooth transition from a given physical dominance to another one.

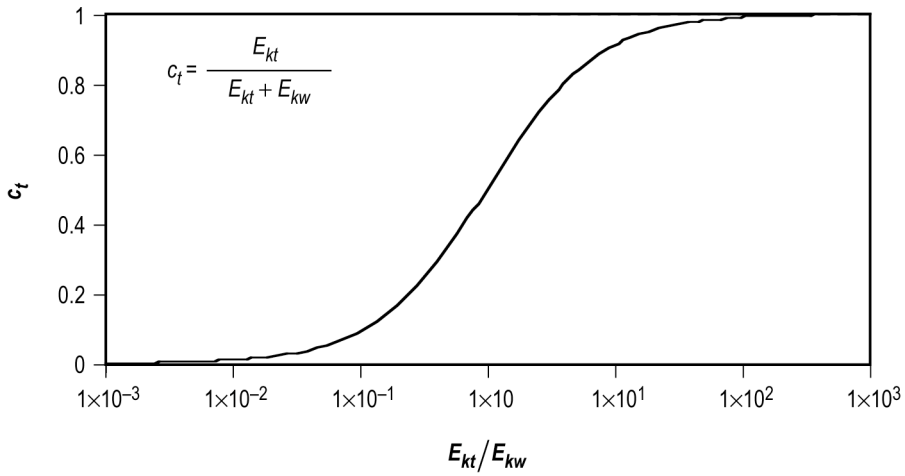

Figure 4. Variation of c_t in terms of τ_w/τ_t .

Since the weighting coefficients represent degrees of the contributions of a particular physical phenomenon to the overall one, it is logical to assign a unity relation between them as

$$c_w + c_t = 1 \ . \tag{28}$$

With this relation, it is easy to recognize from equation (25) that for the constraint of $E_{kt} \gg E_{kw}$, r_p would become equal to r_t, and vice versa, r_p would approach r_w if $E_{kt} \ll E_{kw}$. In other words, equations (25) and (27) ensure that the condition with a larger kinetic energy would have a more significant effect on the atomization process.

Since the framework of the present model closely follows that of the Reitz model, the velocity and properties of the product drops in the present model are formulated in the same manner as the one shown in his model. In each breakup event, product drops are given the same fluid properties and physical location as the parent ones. For the velocity, the product drops would carry the same velocity (V) of the parent along with two additional normal velocity components (v) and (w) in reference to the trajectory of the parent drop. They are represented by

$$\begin{aligned} v &= |V|\tan(\theta/2)\sin\phi \\ w &= |V|\tan(\theta/2)\cos\phi \ , \end{aligned} \tag{29}$$

where

$$\tan(\theta/2) = A_1 \Lambda\Omega/U.$$

A random parameter (ϕ) is chosen on the interval (0, 2π). According to Reitz and Bracco, the constant (A_1) depends on the nozzle design.[40] Its value is set equal to $A_1 = 0.188$ for the present study.

3.4 Turbulent Kinetic Energy of Product Drop

Along with the inclusion of turbulence effect on the primary atomization process, the subject phenomenon is also considered in the secondary droplet breakup model, which is discussed in section 4. At any rate, this new model requires the initial velocity fluctuation quantity of the product drops right after their formation. This quantity can be obtained by examining the energy conservation during the primary breakup process.

When denoting a_{be} and a_{af} as the radii of the parent drop before and after its liquid stripping, respectively, the amount of the mass stripped from the parent drop is formulated as

$$m_{br} = \frac{4}{3}\pi\rho_l\left(a_{be}^3 - a_{af}^3\right) \ . \tag{30}$$

During this breakup process, the change in the individual energy forms of the parent drop is estimated as follows:

Energy due to surface wave motion: $\left(\Delta E_w\right)_{par} = m_{br}\left(\Lambda\Omega\right)^2$

Surface tension energy: $\left(\Delta E_{surf}\right)_{par} = 2\pi\sigma\left(r_{be}^2 - r_{af}^2\right)$

Turbulent kinetic energy: $\left(\Delta E_{tur}\right)_{par} = m_{br}\left(\frac{L_t}{\tau_t}\right)^2$

Kinetic energy of motion: $\left(\Delta E_k\right)_{par} = m_{br}\frac{V^2}{2}$.

For the product drop, the energy associated with the surface distortion is negligible, as compared to the other energy forms, since the initial disturbance is small. Hence, the energy of the product drop is composed of surface tension, turbulence, and kinetic motion as

Surface tension energy: $\left(E_{surf}\right)_{prod} = N_{prod}2\pi r_p^2$

Kinetic energy of motion: $\left(E_k\right)_{prod} = m_{br}\frac{V_{prod}^2}{2}$,

where

V_{prod} = velocity of product drops
N_{prod} = number of product drops

The number of product drops (N_{prod}) is obtained from equation (29) while V_{prod} is calculated from the stripped mass (m_{br}) as

$$V_{prod} = \sqrt{v^2 + w^2} \quad , \tag{31}$$

$$N_{prod} = \frac{3m_{br}}{4\pi\rho_l r_p^3} \quad . \tag{32}$$

By equating the change in the energies of the parent drop with the energy of the product drops, the turbulent kinetic energy for the product drop is written as

$$\left(E_{tur}\right)_{prod} = \frac{\left(\Delta E_w\right)_{par} + \left(\Delta E_{surf}\right)_{par} + \left(\Delta E_{tur}\right)_{par} + \left(\Delta E_k\right)_{par} - \left(\left(E_{surf}\right)_{prod} + \left(E_k\right)_{prod}\right)}{N_{prod}} \quad . \tag{33}$$

Equation (33) is used to determine the initial turbulent kinetic energy for the secondary breakup process.

4. MODELING OF TURBULENCE EFFECT ON SECONDARY DROPLET BREAKUP

This section focuses on the formulation of a term to account for the turbulence motion in the secondary droplet breakup (TTAB), and the method of estimating the initial turbulence quantities used in the TTAB secondary atomization model. The well-known k-ε model is employed in the derivation, and its initial values are estimated based on the parent drop formation. The turbulence intensity within the drops decays as they break up into smaller drops and travel downstream. A criterion of eliminating the turbulence consideration in the secondary breakup process is also formulated in this section.

4.1 Turbulence Term in Secondary Droplet Breakup Model

Studies of the turbulence effect on the liquid breakup suggest that the turbulence motion tends to weaken the surface tension force.[16] In fact, it is well recognized that this surface tension keeps the liquid drop from being torn off, while the turbulence within the drop promotes the droplet disintegration process. To account for this behavior, a term (F_t) is introduced to the right-hand side of equation (12) representing a force associated with the effect of the turbulence on the droplet breakup as

$$m\ddot{\xi} = F + F_t - k\xi - d\dot{\xi} \quad . \tag{34}$$

It is assumed that a portion of the internal liquid turbulence energy forms the turbulence force (F_t). Another portion of subject energy decays through a normal dissipation process. This proposition is based on the experience that turbulence motion behaves like a force participating in the droplet surface deformation and accelerating its surface displacement. Hence, it is proposed that the product of the turbulence force and the deformation rate of the droplet surface displacement must be related to the dissipation rate of the turbulence energy during this breakup process. This relationship is formulated as

$$F_t\dot{\xi} = C_t m\varepsilon \quad . \tag{35}$$

The dissipation rate of the turbulent kinetic energy per unit mass of individual drops is ε and an empirical constant representing the proportionality of subject relationship is C_t.

It should be noted that without additional turbulence generation, the internal turbulent kinetic energy would decay with time as the drops travel downstream. With an assumption of the turbulence within the drop being homogenous and isotropic, the well-known k-ε model that describes the relation between the turbulent kinetic energy (k) and its dissipation rate (ε) can be simplified as follows:[41]

$$\frac{dk}{dt} = -\varepsilon \text{ and } \frac{d\varepsilon}{dt} = -c_\varepsilon \frac{\varepsilon^2}{k}, \text{ with } c_\varepsilon = 1.92 \quad .$$

Knowing the initial turbulent kinetic energy and the initial dissipation rate, denoted as k_0 and ε_0 respectively, k can be expressed with a function of time as follows:

$$k = \left[\frac{\varepsilon_0}{(k_0)^{C_\varepsilon}} (1 - c_\varepsilon) t + (k_0)^{(1-C_\varepsilon)} \right]^{1/(1-C_\varepsilon)} . \tag{36}$$

The derivation of equation (36) is shown in appendix A. It should be noted that k_0 and ε_0 are determined immediately after each droplet breakup process. The expression of ε can now be determined by taking a derivative of equation (36) with respect to time as

$$\varepsilon = -\frac{dk}{dt} = -\frac{\varepsilon_0}{k_0^{C_\varepsilon}} \left[\frac{\varepsilon_0}{(k_0)^{C_\varepsilon}} (1 - c_\varepsilon) t + (k_o)^{(1-C_\varepsilon)} \right]^{C_\varepsilon/(1-C_\varepsilon)}$$

or

$$\varepsilon = \varepsilon_0 \left[\frac{k}{k_0} \right]^{C_\varepsilon} . \tag{37}$$

The turbulence force, shown in equation (35), can be rearranged and written as

$$\frac{F_t}{m} = C_t \varepsilon_0 \left[\frac{k}{k_0} \right]^{C_\varepsilon} \dot{\zeta}^{-1} . \tag{38}$$

By substituting equation (38) and the formulations of coefficients defined in equation (12) into equation (34), this equation becomes

$$\ddot{\zeta} = C_F \frac{\rho_g}{\rho_l} \frac{W^2}{r_p} + C_t \varepsilon_0 \left[\frac{k}{k_0} \right]^{C_\varepsilon} \dot{\zeta}^{-1} - C_k \frac{\sigma}{\rho_l r_p^3} \zeta - C_d \frac{\mu_l}{\rho_l r_p^2} \dot{\zeta} . \tag{39}$$

Again, k is a function of time and is determined from equation (36), whereas C_t is based on available experimental data. The discussion of estimating C_t is presented in section 5. When the distortion displacement (ζ) is nondimensionalized by $y = \zeta / C_b r_p$, equation (39) can be written in a similar form to equation (13) as

$$\ddot{y} = \frac{C_F}{C_b} \frac{\rho_g}{\rho_l} \frac{W^2}{r_p^2} + C_t \frac{\varepsilon_0}{C_b^2 r_p^2} \left[\frac{k}{k_0} \right]^{C_\varepsilon} \dot{y}^{-1} - C_k \frac{\sigma}{\rho_l r_p^3} y - C_d \frac{\mu_l}{\rho_l r_p^2} \dot{y} . \tag{40}$$

Except for the second term on the right-hand side, equation (40) is the same as the governing equation of the TAB model. As stated in section 2, the TAB model has an exact analytical solution. In contrast, the exact solution of the present model cannot be obtained since it has a form of a nonlinear and nonhomogenous differential equation. Therefore, a second-order central finite difference scheme will be

used to solve this equation. The implementation of this model in the numerical calculation is described in section 5.

A similar method, as used in the TAB model, is employed to estimate the postbreakup drop size. The SMR (r_{32}) of the new drops is determined from the energy balance between the parent and product drops. Derivation of the SMR was presented in section 2. Its formulation is shown here for completeness:

$$\text{SMR} = \frac{4\pi r_p^3 \sigma}{E_{par} - \frac{\pi}{6} r_p^5 \rho_l \dot{y}^2} \quad .$$

The total energy of the original drop prior to the breakup (E_{par}) is determined from equation (17).

4.2 Estimation of Initial Turbulence Quantities

The secondary breakup process is considered for all drops created from either the primary breakup or previous secondary droplet breakup and needs initial values of the turbulent kinetic energy and its dissipation rate. These initial turbulence quantities of drops are estimated differently depending on the original formation of the drop.

When a drop is created from the secondary atomization, it is assumed that the turbulence quantities of the parent drop are preserved and distributed evenly to its children drops. The turbulent kinetic energy (k_{bt}) and corresponding dissipation rate (ε_{bt}) of the parent drop at the breakup time are determined from equations (36) and (37). The time and initial turbulence values used in these equations are referenced to the time when the considered drop is formed. Formulations employed for this calculation are

$$k_{bt} = \left[\frac{\varepsilon_0}{(k_0)^{C_\varepsilon}} (1 - c_\varepsilon) t_{bt} + (k_0)^{(1-C_\varepsilon)} \right]^{1/(1-C_\varepsilon)} \tag{41}$$

and

$$\varepsilon_{bt} = -\frac{\varepsilon_0}{k_0^{C_\varepsilon}} \left[\frac{\varepsilon_0}{(k_0)^{C_\varepsilon}} (1 - c_\varepsilon) t_{bt} + (k_0)^{(1-C_\varepsilon)} \right]^{C_\varepsilon/(1-C_\varepsilon)} \quad . \tag{42}$$

Again, t_{bt}, k_0, and ε_0 in equations (41) and (42) are the breakup time and the initial turbulence quantities of the parent drop. Based on the conservation of mass, the initial turbulent kinetic energy and dissipation rate of the new drop are simply formulated as

$$k_0 = \frac{r_p^3}{\mathrm{SMR}^3} k_{bt} \tag{43}$$

and

$$\varepsilon_0 = \frac{r_p^3}{\mathrm{SMR}^3} \varepsilon_{bt} \quad . \tag{44}$$

It should be emphasized that k_0 and ε_0 are denoted for the initial turbulence quantities of a corresponding drop type. The parameters in equations (41) and (42) belong to the parent drops, while they are for the product drops when used in equations (43) and (44).

When a drop of interest is directly produced from the primary atomization, its initial turbulence energy is determined from the energy conservation of the blob drop and its product drops at the breakup time. Formulation of the initial turbulent kinetic energy for the product drop, denoted as $(E_{tur})_{prod}$, has been derived and already presented in equation (33). Hence, the initial turbulent kinetic energy (k_0) per unit mass for the drop is represented by

$$k_0 = \frac{3}{4\pi r_p^3 \rho_l} \left(E_{tur}\right)_{prod} \quad . \tag{45}$$

In their studies of the turbulence droplet breakup, the authors have observed that the turbulence characteristic length scale (L_t) has the same order of magnitude as the product drop size.[41] Therefore, the product drop diameter is selected from the length scale of the initial turbulence in the present study. The initial dissipation rate of the turbulence energy (ε_0) is then determined from the relationship of the turbulence parameters as follows:

$$L_t = C_\mu \frac{k_0^{3/2}}{\varepsilon_0}, \text{ where } C_\mu = 0.09 \quad .$$

When $L_t = 2r_p$, ε_0 can be written as

$$\varepsilon_0 = C_\mu \frac{k_0^{3/2}}{2r_p} \quad . \tag{46}$$

It should be emphasized that equations (45) and (46) are used for estimating the turbulence values of the new drops for the primary breakup only.

4.3 Criterion of Terminating Turbulence Consideration

In a normal atomization process, without consideration of droplet coalescence, the liquid drop breaks up into smaller drops. As a drop travels downstream its size reduces to the smallest possible dimension, and the turbulence activity within the drop also decays. Subsequently leading to conditions in which the turbulence approaches its energy cascade regime. Here, the molecular viscosity is effective in dissipating the turbulent kinetic energy, and the turbulence scales also reduce to the order of the Kolmogorov scale magnitude.[42] For these circumstances, the effect of turbulence on the droplet atomization is no longer necessary since the product drop diameter is either equal to or less than the integral length scale, that is approximately equal to four times the turbulence length scale.[43] Obviously, this length scale is equal to the Kolmogorov length scale in this limit. Hence, a criterion for eliminating the turbulence term in equation (40) is postulated as follows:

$$\text{SMD} \le 4\left[\frac{\mu_l^3}{\rho_l^3 \varepsilon_0}\right]^{1/4} . \tag{47}$$

The bracketed term with its exponent represents the Kolmogorov length scale. It is based on the liquid properties and the initial dissipation rate of the turbulence energy of the new drop immediately after droplet breakup. When the expression above is valid, the turbulence activity of the new drop is no longer effective, and the present model would become the same as the classical TAB model. As seen from the results of all test cases in this study, the new drop size reaches the Kolmogorov scale in about two or three cycles of breakup steps.

The proposed Tblob and TTAB models, along with their KH and TAB counterparts, are used to simulate various flow test conditions. Their predictions are assessed by comparing the analytical results with the measured data. Numerical implementation of these models is described in section 5.

5. NUMERICAL IMPLEMENTATION OF ATOMIZATION MODELS

The first part of this section describes two computer program modules written to evaluate the present models. The proposed finite difference schemes of the Tblob and TTAB governing equations are formulated here, and modeling simplifications used in the program are stated. Other KH and TAB atomization models are used to compare result variations. The last portion of this section covers the implementation of these two physical atomization models into an existing CFD program. The discussion includes numerical techniques of solving the models, simulated physical domain, and computational grid mesh. Sensitivity studies of solution dependency on the computational grid size and selected incremental time steps are also presented.

5.1 Computation of Tblob and TTAB Models for Simple Flow Conditions

Prior to integration of the proposed models into the existing CFD code, two computer programs were written in FORTRAN language to examine the Tblob and TTAB models for simple flow conditions, in which the liquid jet is injected into a quiescent gaseous ambient environment. Listings of these FORTRAN programs are presented in reference 61. The codes track the breakup of an isolated liquid droplet as it travels downstream. Fluid properties, initial velocity, and size of the liquid droplet along with gaseous conditions such as viscosity, pressure, and temperature are specified and assumed constant with time and space. No turbulence in the gas phase is considered for this computation. On the other hand, turbulence inside the liquid drop is considered within the present models. Although the programming is simple and convenient, this framework offers a powerful way to fully assess subject models and compare their predictions with the results of the existing atomization models.

For the primary atomization, the relative velocity between the liquid phase and the local gas flow is approximated using the liquid injection velocity. This assumption is reasonable for analyzing this breakup regime since this phenomenon occurs mostly near the injector exit. A single blob (parent) drop is computed from the injection nozzle exit until it is completely broken up into the children (product) drops. The parent drop size changes with time according to equation (20). This atomization process will produce the children drops and their size is determined from equation (26). Other formulations for the model closure were presented in section 3.

For the secondary droplet breakup, the TTAB model is used to analyze the atomization process of a single drop in a quiescent flow. The governing equation of the TTAB model is solved using a second-order finite difference method. Its formulation is shown in the next section. Drop collision and coalescence are not included in this calculation; however, they are fully incorporated in the CFD simulation. In contrast to the primary breakup treatment, a temporal variation of relative velocity between the drop and gas phase is computed for the secondary atomization. Hence, the individual force terms in the governing equation can be calculated in a more accurate fashion.

The code for the secondary breakup is composed of two parts. The first part determines the coefficient (C_t) shown in equation (35). The drop-size correlation formulated from shock tube experiments,

conducted by Chou et al., is employed to estimate C_t.[44] In the experiments, the breakup of a single liquid drop in a flow behind a moving shock is investigated. The average product drop SMR of the entire secondary breakup process and the parent drop axial velocity (u_p) are collected and reported in the following correlations:

$$\frac{\mathrm{SMR}}{r_p} = 2.6\frac{t_{bt}}{t^*}\left[\frac{\rho_l}{\rho_g}\right]^{1/4}\sqrt{\frac{\mu_l}{2\rho_l r_p W_0}}\ , \tag{48}$$

and

$$u_p = 3.75\frac{t}{t^*}\sqrt{\frac{\rho_l}{\rho_g}}\ . \tag{49}$$

The characteristic breakup time (t^*) is defined as $2r_p\sqrt{\rho_l/\rho_g}\,/W_0$. The time (t) is referenced to the time at which the drop is introduced to the flow field, while t_{bt} is the time when the secondary breakup is complete. Results from the subject experiment suggest that $t_{bt}/t^* \cong 5.5$. Therefore, this value is used in equation (48) for estimating the SMR of the product drops. The initial radius and relative velocity of the parent drop with respect to the gas flow are r_p and W_0, respectively. The relative velocity of the parent drop was computed from equation (49). The result of C_t, presented in section 6, has a value of 0.19. Subsequently, this value is selected for the turbulence constant used in this study.

The second part of this code is used to conduct parametric studies for the test cases listed in table 1. Since drops are injected into the ambient gas, the relative velocity is then calculated from the following relationship:

$$\frac{dW}{dt} = -\frac{3C_D\rho_g}{8r_p\rho_l}W^2\ . \tag{50}$$

The drag coefficient (C_D) is determined from a model offered by Liu et al.[45] In this model, the drag of a deformed droplet is composed of two parts. The first part is the drag of a rigid sphere, while the second part involves drag associated with drop surface deformation. The relationship is represented as

$$C_D = \begin{cases} \dfrac{24}{Re}\left(1+\dfrac{1}{6}Re^{2/3}\right)\left(1+2.632y\right) & Re < 1{,}000 \\ 0.424\left(1+2.632y\right) & Re > 1{,}000 \end{cases}\ . \tag{51}$$

The Reynolds number (Re) is defined as $2\rho_g W r_p/\mu_g$. Droplet distortion displacement (y) is calculated from equation (40). When the value of C_D is computed from a previous time step, equation (50) becomes an ordinary differential equation and can be conveniently solved.

5.2 Implementation of Atomization Models to a Computational Fluid Dynamics Code

For further evaluation, the present models are incorporated into the CFD-ACE+ program, a commercially available software developed by CFD Research Corporation, now owned and marketed by the ESI Group. This code, together with its liquid spray module, solves the equations of steady state as well as transient flow with chemically reactive fluid dynamics and droplet spray. The governing equations and numerical solution method are discussed in the associated software manual and are only described briefly here.[50]

The Navier-Stokes equations and renormalized group (RNG) k-ε turbulence model for a gas phase are solved with a finite volume method. A time marching with a high-order accurate explicit scheme is employed in the transient calculation. With an assumption of dilute spray, parcels of drops are tracked in a Lagrangian framework. The parcel represents an ensemble of identical drops occupied in the same space at a given time. Subsequently, the spray properties at each point are described by statistically sampling the spray parcels. The drop parcels exchange mass, momentum, and energy with the gas through source terms in the Navier-Stokes equations.

It should be noted that CFD-ACE+ uses the classical KH and TAB models to predict the primary and secondary breakup, respectively. For this study, the existing code is modified to incorporate the Tblob and TTAB models.

5.2.1 Tblob Model in Numerical Simulation

As stated in section 2, the liquid is assumedly injected in a form of blob parcels containing spherical drops with their initial size equal to the nozzle exit dimension. The computational approach for the primary atomization proposed by Reitz is adopted in the present study.[22] Extra relations representing the turbulence are described here. Initial turbulence quantities are estimated based on equations (21) and (22). Values of the turbulence characteristic scales are then calculated from these turbulence values. Individual parcels, as described in reference 22, are tracked at each time step, and its drop size is determined using equation (20). Next, the mass stripped from the parent drops is computed and is formed into a new product drop parcel. Primary breakup of the blob drops continues until their size reduces to the dimension of the product drops.

It is not necessary to create a new parcel in each computational time step. To save computer memory and computational time, the stripped mass is accumulated until certain criteria are met. A new parcel is then added to the computations and its drop size is calculated from equation (25). The criterion of forming a new parcel varies among authors. For instance, Reitz defined the creation of a new parcel as when the accumulated mass had exceeded 3 percent of the original parcel mass; while Huh et al. used the value of 10 percent. It was found for the test cases of interest, at least, that the computational results from theses two criteria are not much different, although the number of parcels in the computational domain varies considerably. In CFD-ACE+, a new parcel is created when the number of product drops is greater than 20 percent of the ones in the parent. In the present study, the initial turbulent kinetic energy of the product drops is estimated from the energy conservation formulated in equation (33) and subsequently equation (45). When this estimated energy is less than 0.1 percent of the kinetic energy of the droplet motion, it is assumed that the turbulence motion within the droplet becomes insignificant. No turbulence is considered in the secondary breakup for the subject droplet and the classical TAB model is

employed. Otherwise, the drops would be considered for secondary breakup with turbulence effects that are described in the next part of this section.

5.2.2 TTAB Model in Numerical Simulation

While the parcels produced from the primary atomization are continuously tracked in the Lagrangian coordinate system, they are also considered for the secondary breakup that is governed by equation (40). This equation is solved in the same way as the classical TAB model but it uses the finite difference method since its exact analytical solution does not exist.[23]

To develop the finite difference formulation for equation (40), it is convenient to define a new set of coefficients as follows:

$$C_1 = \frac{C_F}{C_b}\frac{\rho_b}{\rho_l}\frac{W^2}{r_p^2}$$

$$C_2 = C_t \frac{\varepsilon_0}{C_b^2 r_p^2}\left[\frac{k}{k_0}\right]^{C_\varepsilon}$$

$$C_3 = C_k \frac{\sigma}{\rho_l r_p^3}$$

and

$$C_4 = C_d \frac{\mu_l}{\rho_l r_p^2} \ .$$

By substituting the above coefficients, equation (40) becomes

$$\ddot{y} = C_1 + C_2 \dot{y}^{-1} - C_3 y - C_4 \dot{y} \ . \tag{52}$$

In contrast to the TAB model, an exact solution cannot be obtained for equation (40) since it contains the extra term $C_2\dot{y}^{-1}$. Instead, the values of $\ddot{y}$ and $\dot{y}$ can be approximated with a second-order finite central difference scheme in a time step (Δt)

$$\frac{y^{n+1} - 2y^n + y^{n-1}}{\Delta t^2} = C_1 + C_2\left(\dot{y}^n\right)^{-1} - C_3 y^n - C_4 \frac{y^{n+1} + y^{n-1}}{2\Delta t} \ . \tag{53}$$

To calculate y for the next time step, equation (53) can be rearranged as

$$y^{n+1} = \frac{2\Delta t^2 C_1}{2 + \Delta t C_4} + \frac{2\Delta t^2 C_2}{2 + \Delta t C_4}\left(\dot{y}^n\right)^{-1} + \frac{4 - 2\Delta t^2 C_3}{2 + \Delta t C_4} y^n + \frac{\Delta t C_4 - 2}{2 + \Delta t C_4} y^{n-1} \quad . \tag{54}$$

For the first time step, at which $n = 0$, values of y^0 and $\dot{y}^0$ must be given, and y^{-1} (that is, the value of y at $n = -1$) must be defined. Furthermore, the first-order backward differencing formulation can be used to estimate y^{-1} as

$$\dot{y}^0 = \frac{y^0 - y^{-1}}{\Delta t} \Rightarrow y^{-1} = y^0 - \Delta t \dot{y}^0 \; .$$

Since an initial displacement of droplet deformation and its time derivative are not known for most simulation cases, they can be assumed to be equal to zero. Deformation displacement (y) is computed at every time step. The secondary breakup assumedly occurs when y approaches 1. The product drop size is then calculated from equation (19). At the same time its initial turbulence quantities are estimated from equations (43) and (44).

Again, the new product drops are continuously tracked for possible future secondary atomization until they leave the computational domain. When the product drop size is smaller than the Kolmogorov length scale, equation (47), the turbulence activity of the new drop is no longer considered. In this case, the present model would become the same as the classical TAB model.

5.2.3 Implementation of Collision/Coalescence

In the study of the liquid fuel jet breakup, Hiroyasu and Kadota observed that large drops appear on the central part of the spray when injecting the liquid with the small spray angle, as defined in section 6.[46] Their conclusion was that the large drop results from the collision and coalescence processes inside this region. Hence, it is necessary to include these behaviors in the modeling of the liquid spray. For this study, a program routine was written to compute the drop collision and coalescence model suggested by O'Rourke.[51] Details of the subject model can be found in reference 51.
A brief review of this model is presented here.

The collision frequency (υ_{12}) of droplets contained in any parcel pairs, denoted as parcels 1 and 2, within each computational cell is examined. This frequency is expressed as

$$\upsilon_{12} = \frac{N_2}{Vol}\pi\left(r_1 + r_2\right)^2 \left|v_1 - v_2\right| \; . \tag{55}$$

Subscripts 1 and 2 denote drops with a large radius (r_1) and a small radius (r_2). The parameter (N_2) is the number of drops in parcel 2, v denotes the drop velocity vector, and Vol represents the volume of the cell. The number of probable collisions (n) between the droplet pair is calculated from the Poisson distribution ($P(n)$) as follows:

$$P(n) = \frac{e^{-\upsilon_{12}\Delta t}\left(\upsilon_{12}\Delta t\right)^n}{n!} \quad . \tag{56}$$

The incremental time (Δt) is the computational time step. The Poisson distribution ($P(n)$) can be stochastically defined from the uniform distribution in the interval (0,1). When any two drops collide, coalescence between them may or may not occur. Therefore, a collision impact parameter (b) is introduced to determine these two possibilities. If b is less than a critical value (b_{cr}), the colliding drops undergo velocity changes, while their sizes are unchanged. This phenomenon is called a grazing collision reflected by

$$b^2 = q(r_1 + r_2)^2 \tag{57}$$

$$b_{cr}^2 = \left(r_1 + r_2\right)^2 \min\left[1, 2.4\frac{\left(r_1/r_2\right)^3 - 2.4\left(r_1/r_2\right)^2 + 2.7}{We_l}\right] . \tag{58}$$

A random number (q) is generated on the interval (0,1). When the value of the impact parameter exceeds its critical value the drops then coalesce. In this case, n would be the number of drops to be taken away from parcel 2. The size and velocity of the new drops must be recalculated according to relations described in reference 51. The computation of the collision and coalescence model is carried out for all parcels of interest at each time step.

It should be noted that a considerable coalescence appears when the difference between r_1 and r_2 is large. Furthermore, the collision and coalescence processes are considered for all drops in this study, except for the blob drops. It is not logical to have the blob drops included in these processes since they are representative of the liquid jet.

5.2.4 Computational Domain and Grid Mesh

Eight computational test cases that are related to experiments conducted by various authors have been selected for the present work. These test cases will be referred to throughout this TM, and their appropriate available measurements and predicted results are presented and compared in section 6. The flow conditions of the cases are summarized in table 1. For Tblob, the turbulence scales, initial turbulent kinetic energy, and dissipation rate are estimated from equations (22) and (24) by knowing the injection nozzle configuration and its flow conditions. Kinetic energy and dissipation rate values are listed in table 1. It should be noted that for some test cases the measured data to calculate the initial turbulence values are not entirely reported. Subsequently, typical values are estimated and utilized in the calculation. Details of determining these initial values are shown in appendix A.

Table 1. Test cases and measured data used in the computations.

Case	H–1	H–2	H–3	Y–1	Y–2	Y–3	K	S
Nozzle diameter (mm)	0.3	0.3	0.3	0.213	0.213	0.213	0.24	0.15
Ambient gas	Nitrogen	Nitrogen	Nitrogen	Carbon dioxide	Carbon dioxide	Carbon dioxide	Nitrogen	Nitrogen
Ambient pressure (MPa)	1.1	3	5	4.5	2.5	0.5	2.17	1.5
Ambient temperature (K)	298	298	298	298	298	298	298	289
Density (kg/m^3)	12.36	33.7	56.17	72.61	40.34	8.07	24.51	16.84
Liquid fuel	Diesel fuel	Diesel fuel	Diesel fuel	Diesel fuel	Diesel fuel	Diesel fuel	Diesel fuel	Diesel fuel
Density (kg/m^3)	840	840	840	840	840	840	840	840
Viscosity (kg/m s)	2.9×10^{-3}	2.9×10^{-3}	2.9×10^{-3}	5×10^{-3}	5×10^{-3}	5×10^{-3}	5×10^{-3}	2.9×10^{-3}
Surface tension (N/m)	2.05×10^{-2}	2.05×10^{-2}	2.05×10^{-2}	2.06×10^{-2}	2.06×10^{-2}	2.06×10^{-2}	2.06×10^{-2}	2.05×10^{-2}
Injection velocity (m/s)	102	90.3	86.41	185.42	185.42	185.42	133.81	183
Initial Turbulence Quantity								
Kinetic energy (m^2/s^2)	2.88×10^{2}	2.26×10^{2}	3.94×10^{1}	1.58×10^{3}	1.58×10^{3}	1.58×10^{3}	5.22×10^{2}	4.64×10^{2}
Dissipation rate of kinetic energy (m^2/s^3)	1.06×10^{8}	7.34×10^{7}	1.22×10^{7}	1.49×10^{9}	1.49×10^{9}	1.49×10^{9}	3.14×10^{8}	6.11×10^{8}
Authors	Hiroyasu and Kodota	Hiroyasu and Kodota	Hiroyasu and Kodota	Yule et al.	Yule et al.	Yule et al.	Koo	Schneider
Reference	46	46	46	47	47	47	48	49

Two-dimensional axisymmetric CFD simulations are performed using CFD-ACE+ to compute the various cases listed in table 1. A physical domain of 100×30 mm in the axial and radial directions, respectively, is discretized into a grid mesh of 41×25 points in the respective directions. As depicted in figure 5, the grid points in this baseline mesh system are clustered near the injector nozzle exit and the centerline. The smallest cell of 0.7×1 mm in the radial and axial directions contains the injection exit port. Boundary conditions used in this numerical simulation are labeled in figure 5.

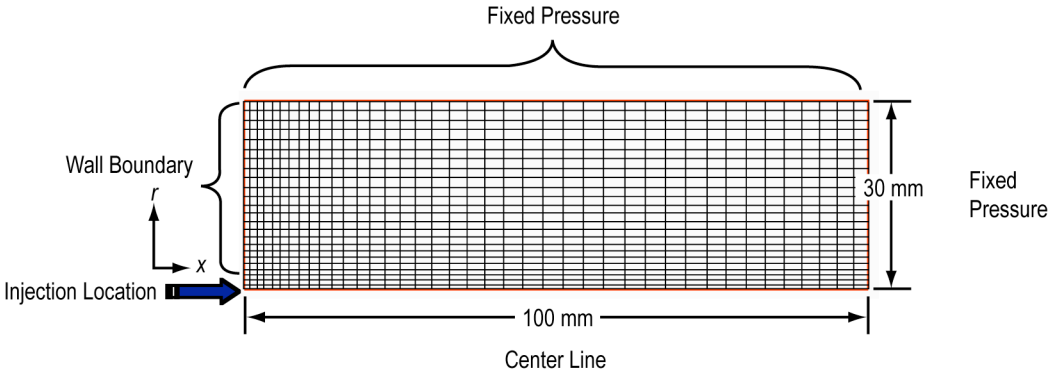

Figure 5. Baseline two-dimensional axisymmetric computational grid mesh.

The liquid jet, in a form of blob drop parcels, is injected into a quiescent gas at the location of $x=0$ and $r=0$. These drops have the same radius as the nozzle exit. They are injected randomly within a prespecified spray angle of the liquid jet at an axial velocity equal to the liquid jet velocity. Although the spray angle sensitivity study is not presented here, the results reveal that the variation in the spray angle

from 8–18° has only some minor effects on the spray tip penetration. Tip penetration is defined as the distance of the parcel that travels the farthest downstream at a given time. With suggestions of various authors, the spray angle of 15° is used for this computation.[24,27]

It is necessary to point out that only a single parcel each time step is injected at the nozzle exit. The number of drops in each initial parcel is determined from the injection mass flow rate, blob drop size, and incremental step time. A longer step time would have a larger number of drops per initial parcel. Subsequently, a computation with a larger step time would carry fewer parcels as compared to one with a smaller step time. However, a large step time may compromise the computational accuracy. For this study, a step time (Δt) of 2.5×10^{-6} s is used. It should be noted that $\Delta t = 2.5\times10^{-6}$ s is selected to have the breakup time of drops at least one order of magnitude larger than the computational step time. Small differences are noticed in the computational results for cases of $\Delta t = 1\times10^{-6}$, 2.5×10^{-6}, and 1×10^{-5} s.

To investigate the solution dependency on the grid mesh, test case H–1 is simulated with four grid mesh sizes of 31×21, 41×25, 61×35, and 81×41. Predicted values of the tip penetrations along with the measured data are plotted in figure 6.

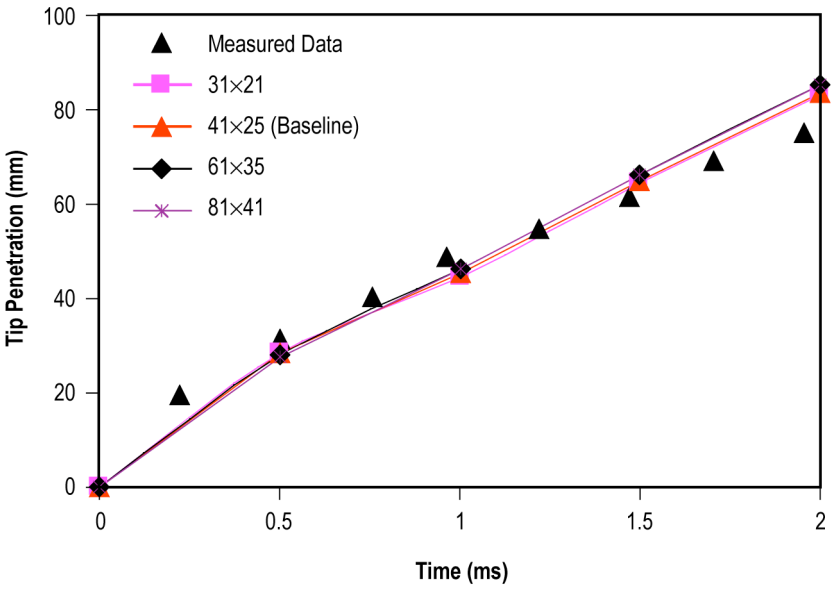

Figure 6. Tip penetration predictions with various grid mesh sizes.

The results indicate that the predicted tip penetrations for all cases are close. In comparison with the experimental data, the numerical simulation slightly underpredicts the penetration length in the first millisecond and overpredicts afterwards. It should be pointed out that, to some degree, the solution dependency on the grid size should be expected, although the present results do not show this trend. In a computational study of liquid jet atomization with the dilute spray assumption, Khosla and Crocker observed that some solution sensitivity on grid mesh does exist.[52] In addition, a very fine grid system

may produce unrealistic results since the dilute spray assumption may no longer be valid. In summary, it is reasonable to select the grid mesh of 41×25 for this study.

Computation results of the present models are discussed further in section 6. Predictions of the present models and the two classical atomization models are compared and discussed. The study results are also appraised against the measured data.

6. RESULTS AND DISCUSSIONS

Prior to implementing the present models into CFD-ACE+, two separate computer routines were written to examine the Tblob and TTAB models for simple flow conditions in which the liquid jet is injected into a quiescent gaseous ambient environment. The predictions of the present models and the two classical atomization models are compared and discussed. The computational results from these codes are presented detail. Predictions of the present models are evaluated against the measured data. Appropriate comparisons with the existing atomization models and results of the numerical simulations are also shown.

6.1 Primary Liquid Jet Breakup Model (Tblob)

As stated in sections 2 and 3, the reduction rate of the parent drop size is governed by equations (11) and (20) for the KH and Tblob models, respectively. These equations also describe the mass stripped from the parent drop as it travels downstream. The term $\left(C_a L_t / \tau_t\right)$ on the right-hand side of equation (20) represents the contribution of turbulence effects on the rate of change in the parent drop size, while the other term $\left(a - C_a L_w\right)/\tau_w$ represents the effects of the surface wave perturbation. The values of these terms for test cases H–1 and H–3 (table 1) can be found in figure 7.

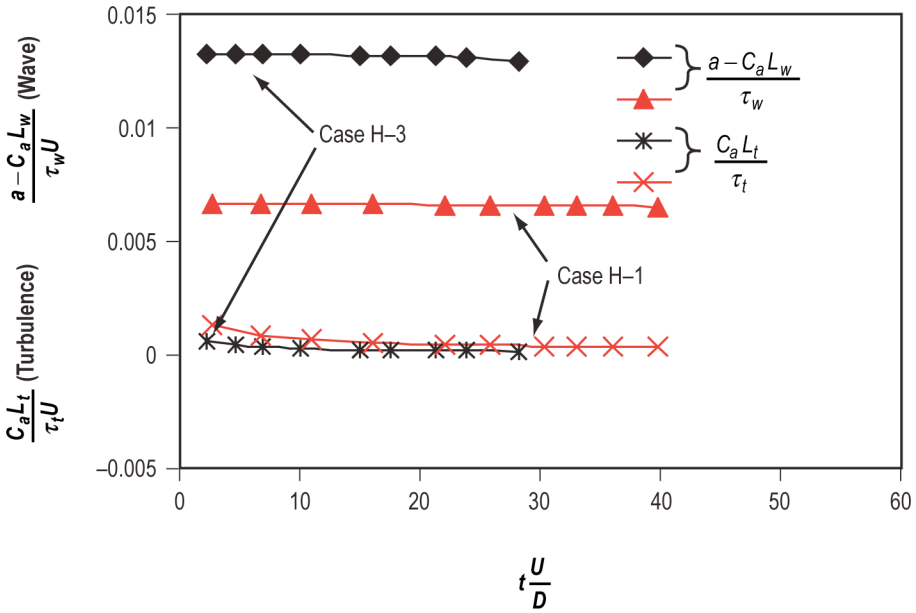

Figure 7. Values of the wave motion and turbulence terms on the reduction rate of the blob (parent) drop size.

In figure 7, the values of these terms are plotted against the relative lifetime of the parent drop. This parameter is nondimensionalized by injection velocity and injection nozzle diameter. Results for the considered cases indicate that the surface wave perturbation has a considerable effect on the reduction rate of the parent drop size. The value of the wave motion term in test case H–3 is approximately two orders of magnitude greater than the turbulence term. However, when the injection velocity increases from 86.4 m/s (case H–3) to 102 m/s (case H–1) the gap of these two values becomes smaller. This suggests that the value of the turbulence term rises at a faster rate than that of the wave motion term when increasing the injection velocity. The reduction rate of the parent drop decreases with the increase of the velocity.

It is evident from figure 7 that the reduction rate in the parent drop size is nearly constant with time. This trend is due to the fact that the term associated with the surface wave motion is determined from the wavelength and its fast growth rate, which are not a function of time. On the other hand, the turbulence term is calculated from equations (21) and (23) that include the time terms. Combining these two equations when calculating the turbulence term only offers a slight decrease in its value with time. In addition, the end of the parent drop breakup occurs in a relatively short time. The results show the rate of change in the parent drop size is almost constant. Therefore, the curves of the parent drop diameters are nearly straight downward, as shown in figure 8. In all test cases, the Tblob model predicts the completion of the parent drop breakup slightly earlier than the KH model.

It should be pointed out that the Tblob model only describes the primary breakup. However, in the actual measurement, it is difficult to separate other physical phenomena such as secondary droplet breakup, etc. Therefore, only the intact core length of the liquid jet can legitimately be used to compare the measurement and prediction. An available correlation of the intact length that has been widely employed in literature is used to compare with the present prediction.[53] The correlation is shown as

$$L_{jet} = C_{jet}\sqrt{\rho_l / \rho_g}\, D\,. \tag{59}$$

The intact length is denoted as L_{jet}, and the constant (C_{jet}) has a value of 10. In recalling the implementation of the KH and Tblob primary breakup models, the liquid jet is injected in the form of blob parcels. When traveling downstream, the blob (parent) drop strips its mass to generate the product drops. This process is completed when the parent drop size is approximately equal to the size of its product drops. Hence, it is reasonable to define the intact length of the liquid jet as the traveling distance of the parent drop during this process. Figure 9 shows the nondimensional intact length L_{jet}/D predicted by the KH and Tblob models, as well as the relationship of equation (59) for all test cases plotted against the square root of the density ratio $\sqrt{\rho_l/\rho_g}$.

The predicted results from the KH and Tblob models reasonably agree with the correlation curve. In general, the data points from the Tblob model are closer to the correlation line in comparison to those from the KH model. Furthermore, the Tblob model predicts a shorter intact length than the KH model. This prediction is consistent with the measured data trends observed by other authors.[8,53]

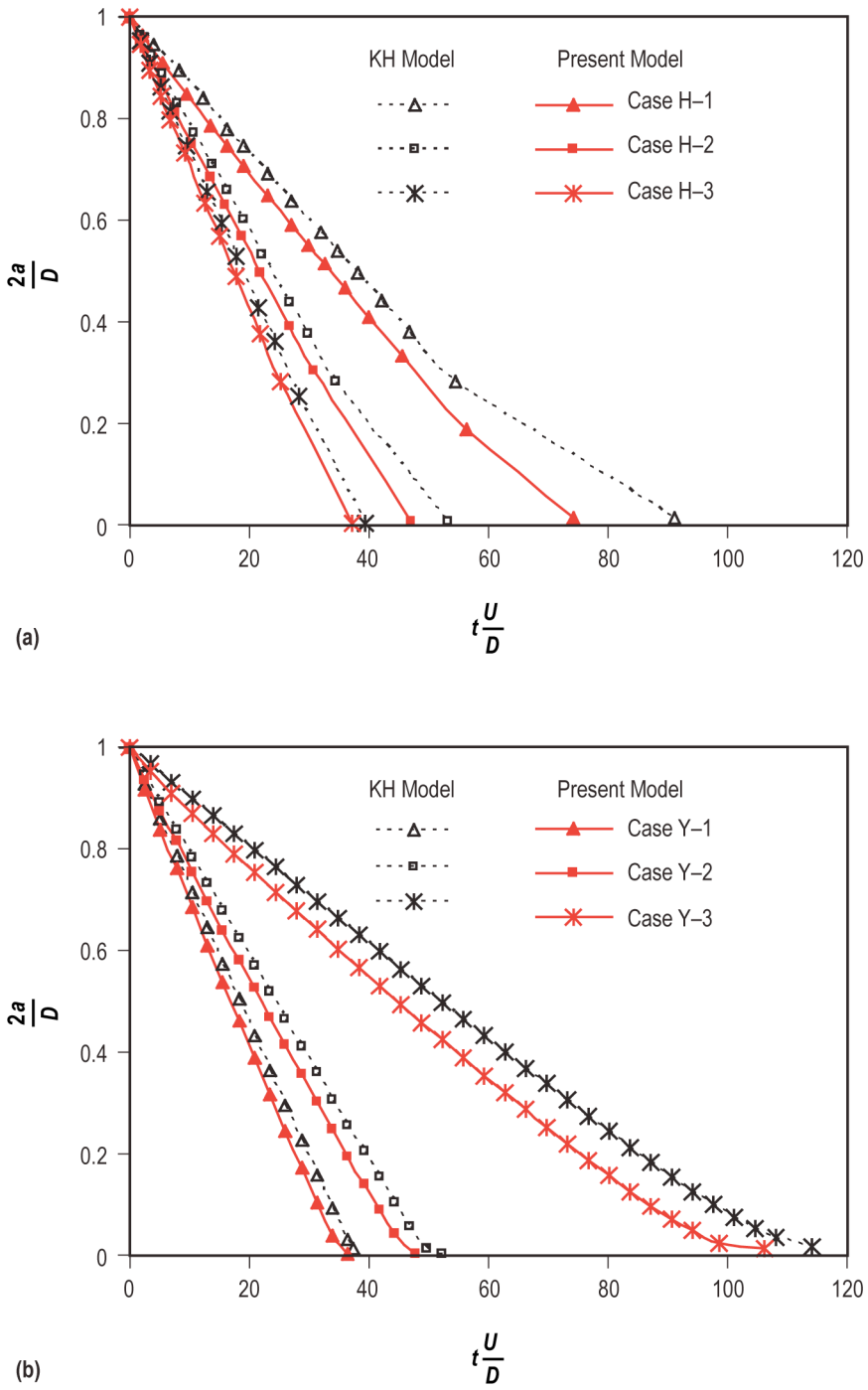

Figure 8. Rate of change in parent drop size predicted by KH and Tblob: (a) Test cases H–1 through H–3, and (b) test cases Y–1 through Y–3.

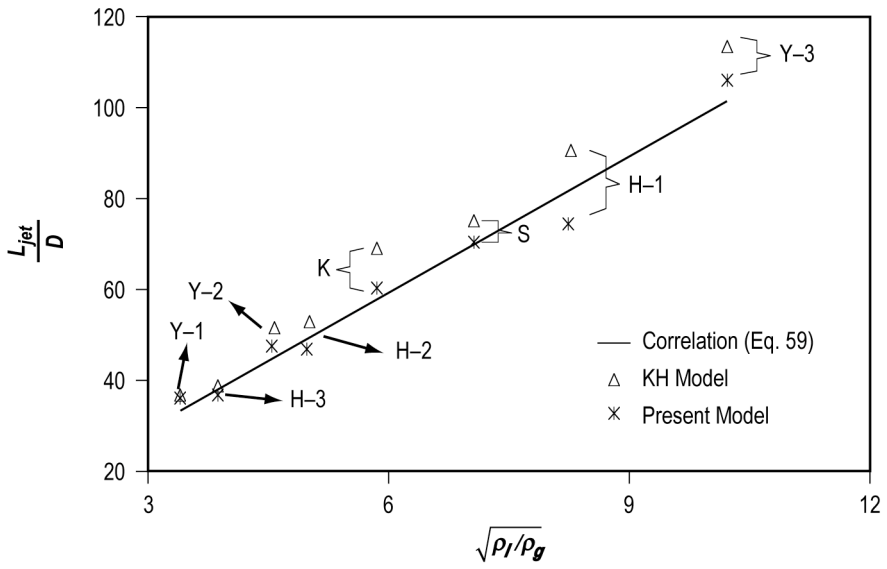

Figure 9. Comparison of predicted and correlation intact lengths of the liquid jet.

In the present model, both the liquid jet surface wave perturbation and the turbulence motion play a part in forming the product drops. Their drop size, as shown in equation (25), is composed of the two radial length scales r_w and r_t. They are weighted by the kinetic energies of the respective phenomena when used to determine the radius of the product drops. The values of subject parameters for test case H–3 are plotted in figure 10. The curve showing the kinetic energy of the surface wave motion (fig. 10(a)) is very much constant with time because the surface wavelength and its corresponding growth rate are not a function of time. On the other hand, kinetic energy associated with turbulence is initially at a high level due to the turbulence developed at the injector nozzle exit. However, its value rapidly decreases through the dissipation process and approaches the level of the surface wave motion. This trend has led to define the weighting coefficient curve, equation (27), as that which starts at the value near unity and then quickly reduces its value to one half at the end of the product drop generation.

Figure 10(b) presents the radial length scales formulated from the two considered motions. Using the same previous argument of the surface wavelength being constant, it is easy to recognize from equation (9) that the radial length scale (r_w) associated with this motion is more or less constant with time. In contrast, the scale (r_t) referring to equation (26) increases with time, since the turbulence length scale (L_t) shown in equation (23) also increases with time. When applying the weighting coefficient (C_t), shown in figure 10(b), in the determination of the product drop size, the resultant value of r_p initially rises and then gradually drops due to the reduction of C_t. This trend can be interpreted such that the high-turbulence intensity at the initial primary breakup stage controls the formation of the product drop size. Turbulence dissipates as the parent drop travels downstream. This drop formation process is then gradually dominated by the surface wave perturbation. For test case H–3, as determined from the Reitz model, r_w has a value less than 1 μm; while r_t, formulated by Huh et al., is approximately 20 μm.[27] Due to neglecting the drop collision and coalescence effects, the value of r_t is more representative of the drop size found in the measured data. The same value is also predicted by the Tblob model at the initial

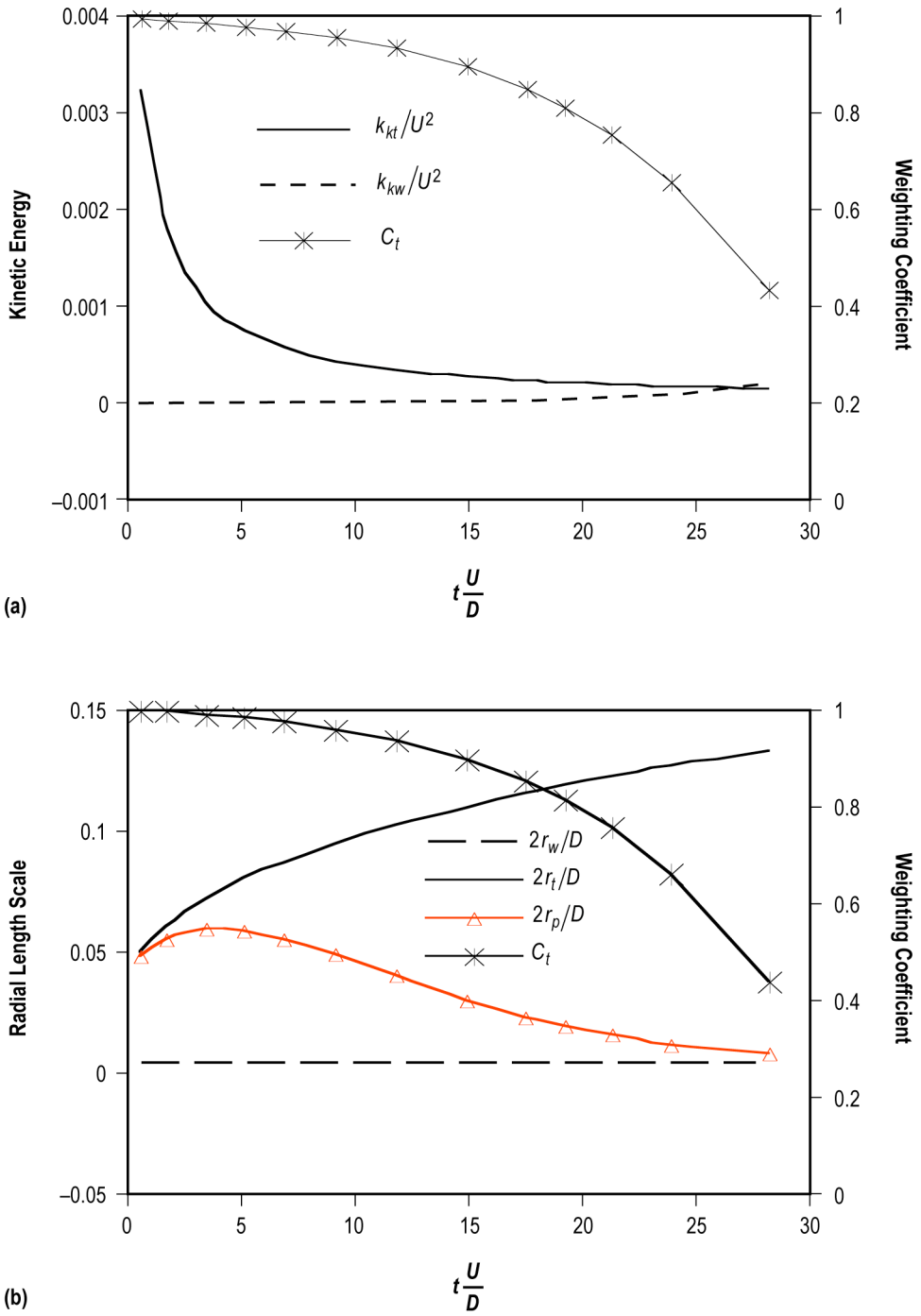

Figure 10. Parameters used to determine product drop size: (a) Kinetic energies and weighting coefficient and (b) radial length scales and weighting coefficient.

product drop formation. However, the drop size continues to decrease to the level predicted by the KH model. As the parent drop strips its mass and consequently reduces its size when traveling downstream without coalescence, it is logical to expect that the product drop size should also decrease in this process.

It should be noted that the same trends of all parameters describing test case H–1 are also observed in all the test cases shown in table 1. The prediction of product drop sizes for test cases H–1 to Y–3 are displayed in figure 11.

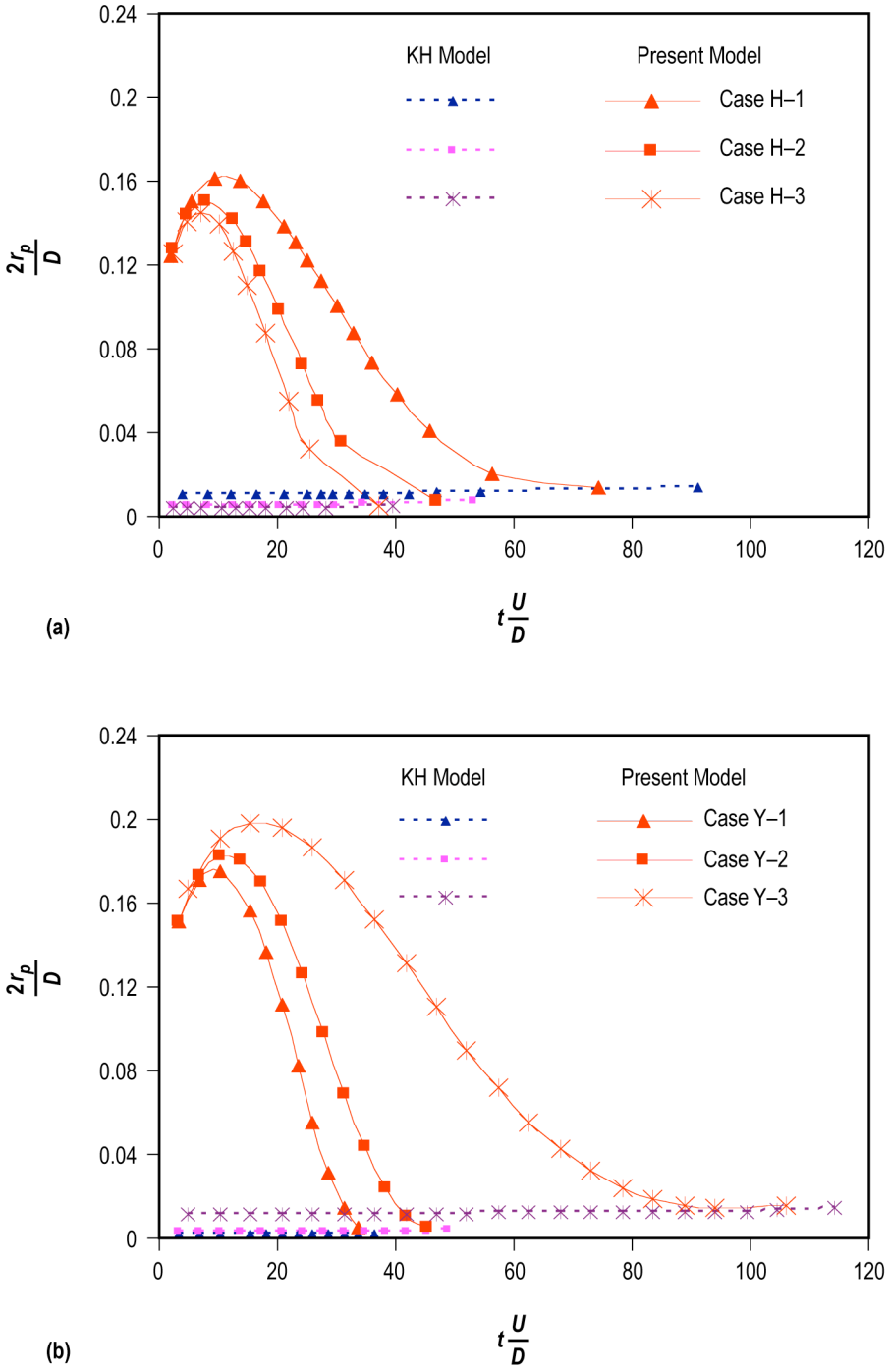

Figure 11. Product drop size predicted by KH and Tblob models: (a) Cases H–1 through H–3 and (b) cases Y–1 through Y–3.

The results indicate that when liquid is injected at a higher velocity (test cases H–1 and Y–1) the product drops are initially formed with a larger size. This product drop formation process is prolonged in comparison to cases of lower injection velocity (test cases H–3 and Y–3). Similar to the observation from figure 10, the results shown in figure 11 reveal that the product drop size predicted from the Tblob model is approximately one order of magnitude larger than the one from the KH model. Again, by ignoring other effects, the drop size estimated from Tblob is consistent with the experimental data. It should be restated that the gaseous flow field as well as drop collision and coalescence are implemented in the CFD simulation. An effect of the initial turbulent kinetic energy on the primary atomization process is also investigated in this study. The purpose here is to assess the sensitivity of the primary atomization due to the different inlet turbulence levels. This is achieved by using various levels of the initial turbulence kinetic energy (k_0) while keeping its dissipation rate (ε_0) constant. Figure 12 portrays the change in the liquid jet intact length (L_{jet}) due to the variation of initial turbulent kinetic energy (k_0).

Percentage values of the change in L_{jet} and k_0, shown in figure 12, are referenced to test case H–3. The results indicate that the initial energy has a considerable influence on the jet breakup. The intact length becomes shorter when increasing the value of k_0. It implies that the higher the initial turbulent energy the faster the primary atomization process accelerates, which leads to an early completion of the breakup. Phinney and Tseng et al. also drew similar conclusions from their experimental observations.[8,14] It should be noted that the curve in figure 12 approaches asymptomatically to the k_0 coordinate for the higher value of k_0. This trend indicates that the initial turbulent energy has a lesser effect on the change in the intact length when this energy further increases.

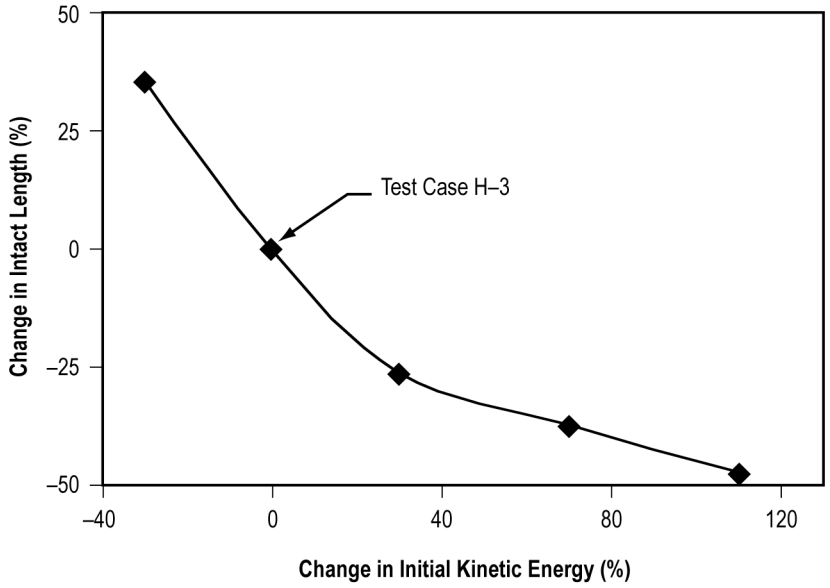

Figure 12. Change in the liquid jet intact length due to variation of the initial turbulent kinetic energy for test case H–3.

As the product drops from the primary liquid jet breakup continue traveling downstream, they are exposed to external as well as internal forces. Subsequently, they may undergo additional breakup cycles. This phenomenon is driven by the secondary breakup mechanism.

6.2 Secondary Droplet Breakup Model (TTAB)

A computer routine was written to assess the secondary droplet breakup model. The code tracks the breakup of an isolated liquid droplet traveling in a gaseous medium. The model is computed with a temporal variation of relative velocity between the drop and the gas medium. Hence, the force terms in the governing equation of the drop breakup process can be predicted in a more realistic manner. The relative velocity relationship used in this computation was discussed in section 5.

6.2.1 Evaluation of Turbulence Force Constant (C_t)

In equation (35), the coefficient (C_t) represents the proportionality between the dissipation rate of the turbulent kinetic energy and the turbulence energy participating in droplet deformation. For the present study, the value of C_t is estimated from measurements of drop breakup provided by Chou et al.[44] In their shock tube experiment, the breakup of a single liquid drop in a flow behind a moving shock wave was investigated. The gas in the driven section flows at a velocity of ≈80.8 m/s with a density of 1.48 kg/m^3. Results from the subject experiment suggest that t_{bt}/t^* is ≅5.5, therefore, this value is used in equation (48) for estimating the SMR of the product drops. For the coding of the secondary breakup models (TAB and TTAB), the relative velocity of the parent drop was computed from equation (49). Due to the lack of measured droplet turbulence quantities, the initial turbulent kinetic energy (k_0) used in TTAB is estimated from the parent drop velocity, equation (40). Based on numerical simulations of primary atomization for the cases listed in table 1, the ratio of the fluctuation velocity within the drop and the drop velocity ranges from 0.09–0.11. Now the ratio of 0.1 is selected for determining the initial droplet turbulence energy. Since Chou et al. and Liang et al. indicated that the drop starts the breakup at $t/t^* = 1.5$, the initial drop velocity is predicted for this particular time.[44,54] The initial dissipation rate (ε_0), required in equation (40), is estimated with the relation shown in equation (46). A single water drop of 590 μ*m* in diameter was analyzed using density, viscosity, and surface tension constants of 997 kg/m^3, 8.94×10^{-4} kg/ms, and 70.8×10^{-3} N/m, respectively. The product drop size for this case at various C_t values is plotted in figure 13.

Since correlation of the experimental data is not related to C_t at all, its value at SMR/$r_p = 0.135$ remains constant, as shown in figure 13. Note that the TAB model does not carry the turbulence term so results from this model would also not vary with C_t. Furthermore, TAB predicts the product drop size at SMR/$r_p = 0.145$, which is roughly 7.5 percent larger than the measured value. The solid line curve in figure 11 displays the results of the present model with a variation of C_t. As would be expected, the TTAB model reproduces the same results of the TAB model when $C_t = 0$. With an increase in the value of C_t, TTAB predicts a smaller product drop size. In other words, results of the present model suggest that the secondary atomization process would create a smaller drop size when stronger turbulence exists within the parent drop. It is evident from the plot that the predicted SMR of the product drop matches the measured data for $C_t = 0.19$. Consequently, this value is selected for the turbulence constant used in this study.

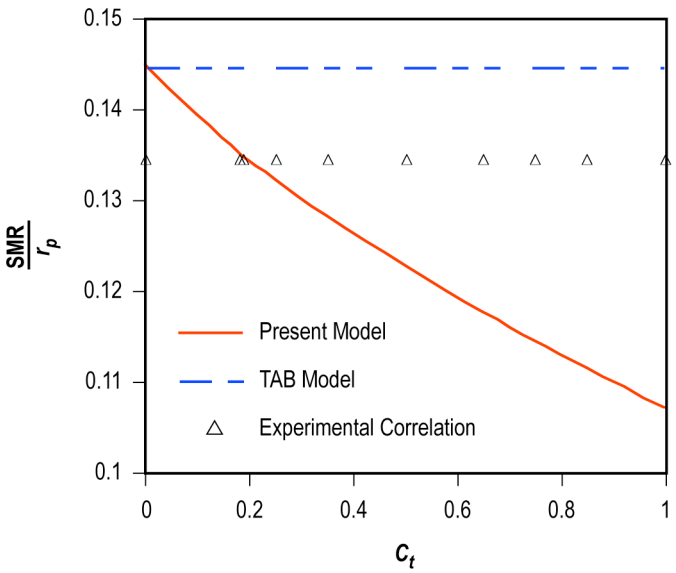

Figure 13. Variation of product drop size due to turbulence force coefficient C_t.

6.2.2 Assessment of TTAB Model

For this particular study, the relative velocity between the drop and the gaseous environment is calculated from equation (50). Since the initial turbulence quantities are required for the TTAB model, it is worthwhile to conduct a sensitivity study of the turbulent kinetic energy (k_0) on the predicted results. Variations of the product drop size and drop breakup time at different $k_0/0.5mW_0^2$ values for test case H–3 in table 1 are plotted in figure 14.

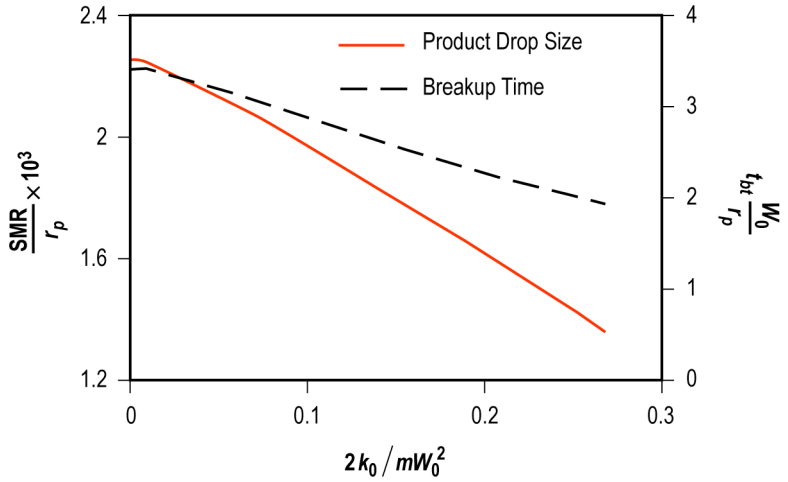

Figure 14. Product drop size and breakup time of various initial turbulent kinetic energies.

The x coordinate represents the ratio of the initial turbulence energy (k_0) and droplet motion kinetic energy $1/2mW_0^2$. Curves of both the product drop size and the breakup time show that these quantities are decreasing almost linearly with an increase of the initial turbulence energy, except for $k_0 \sim 0$. These results suggest that the level of initial turbulence within the liquid has a strong effect on the droplet breakup. It is of interest to note that the secondary atomization process generates smaller drops with the inclusion of turbulence. Also, it takes a shorter time to break up the parent drop when turbulence is considered.

When implementing the secondary atomization model with the CFD code, initial turbulence quantities are estimated from the parent drop formation process, as discussed earlier in section 4. As the CFD results have shown, $k_0/0.5mW_0^2$ ranges from 0.09 to 0.11 for test case H–3 when the drop is formed during the primary atomization. Hence, it is reasonable to assign $k_0/0.5mW_0^2 = 0.1$ for the current study.

From the governing equation (40), droplet distortion motion is driven by the interaction of aerodynamic, turbulence, surface tension, and viscosity events. To show the variation of these quantities with time, their nondimensional values are plotted with time in figure 15.

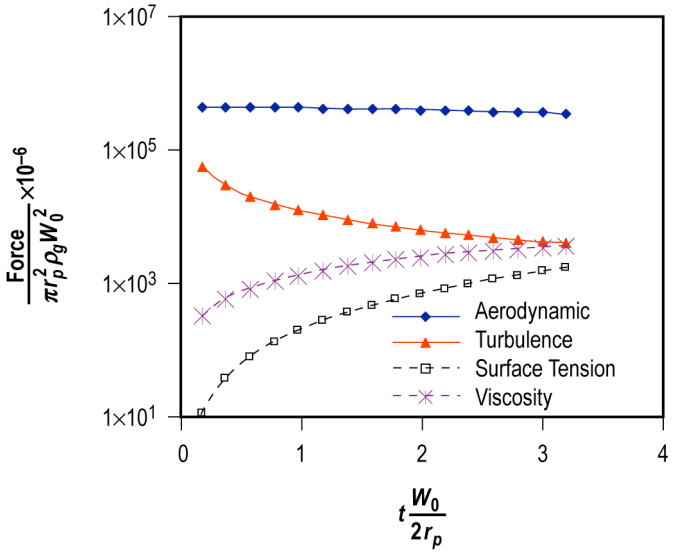

Figure 15. Forces generating droplet distortion based on TTAB.

This plot depicts that the aerodynamic force has a strong effect on the droplet breakup process, which is expected, since the flow conditions for test case H–3 relate to a Reynolds number $\left(2\rho_g r_p W_0/\mu_g\right)$ and Weber number $\left(2\rho_g r_p W_0^2/\sigma\right)$ of 3.8×10^3 and 80.7, respectively. Also, the time derivative of the distortion displacement (y) of figure 14 starts at a small value and increases with time. Since the turbulence force is inversely proportional to the y derivative, this force consequently is very high at the initial time and rapidly changes to a smaller value. In contrast, the surface tension and

viscosity forces are initially small and change to large values with time because they are directly proportional to y and $\dot{y}$, respectively. According to the breakup model for the case without any turbulence, the drop distortion motion is created by the difference of forces between the aerodynamics and the sum of the surface tension and viscosity. Obviously this process is accelerated when turbulence is considered. A comparison of y and $\dot{y}$ computed from TAB and TTAB is presented in figure 16.

The distortion displacement (y) will increase with time when these forces act on the drop. Moreover, an imbalance of these forces leads to an increase in the time derivative of this displacement ($\dot{y}$). When y reaches the value of one, the parent drop produces smaller drops. Figure 16 also reflects a consistency with the results observed in figure 15. Because of an additional turbulence term considered in the TTAB model, it predicts higher values of y and $\dot{y}$ at a given time in comparison to the results of TAB. Subsequently, the breakup time determined from the TTAB model is shorter than the TAB model.

Although no measured data of the secondary breakup are available for the test cases, listed in table 1, they are still computed with both the TAB and TTAB models to assess the variation in their results. Figure 17 shows a comparison of the predictions from TAB and TTAB.

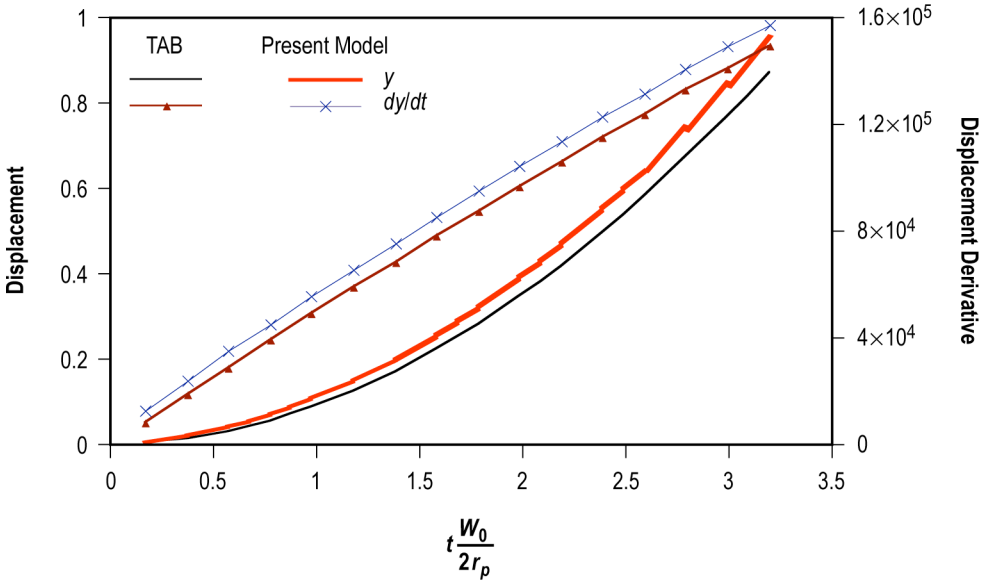

Figure 16. Comparison of the droplet displacement (y) and its derivative ($\dot{y}$) predicted by TAB and TTAB.

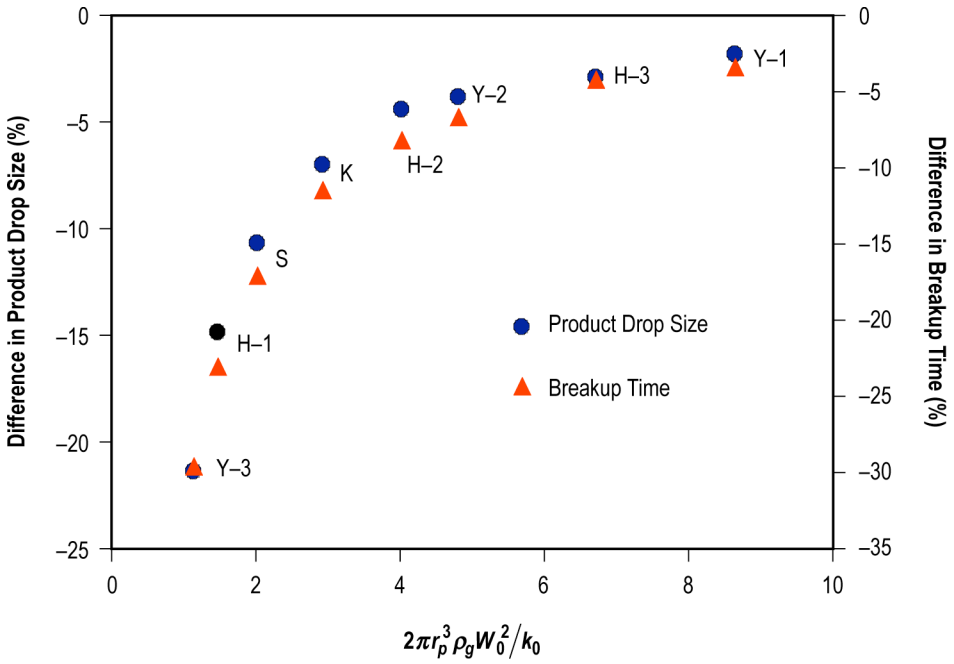

Figure 17. Difference in product drop size and breakup time predicted by TAB and TTAB.

The *x* coordinate of the plot shows the ratio of aerodynamic and turbulence forces. This parameter is selected for plotting since the aerodynamic force is generally dominant in the droplet breakup process. The right and left vertical coordinates represent the percentage differences in the product drop size and breakup time, respectively, as predicted from TAB and the present model. The negative scales of these two coordinates indicate that the present model predicts smaller values. The results also suggest that the large variation of the two predictions appears at the low aerodynamic/turbulence force ratio, where turbulence action becomes significant in comparison to aerodynamic force. However, the variation becomes smaller with an increase of this ratio value, where the aerodynamic force is dominant. This trend suggests that the large variation between the two predictions results from the large turbulence force. When the aerodynamic force is significantly higher it plays a key role in the droplet breakup. For this condition, the results from TAB and TTAB are not much different, regardless of how high the value is of the turbulence force.

For further evaluation, the proposed models are implemented into the CFD-ACE+ software and numerical simulations of the test conditions are performed. These results are presented in section 6.3.

6.3 Computational Fluid Dynamics Numerical Simulation

As described in section 5, the Tblob and TTAB models which represent the primary and secondary atomization processes, respectively, are implemented in CFD-ACE+ for further evaluation. Numerical simulations of several test cases using this code are performed and compared with available measured data. Also, variations in the predictions from the two classical models KH and TAB, which already exist in this code, and the present models are examined.

In this study a two-dimensional axisymmetric flow is simulated with a cylindrical liquid jet located at the centerline. It should be noted that the axisymmetric conditions, which are imposed here, are for mean values associated with the Reynolds averaged Navier-Stokes (RANS) formulation. Although instantaneous turbulence quantities are three-dimensional in nature, the k-ε turbulence model that is used as the baseline model for this study does not account for nonisotropic effects. However, a cylindrical liquid jet dominated by the effective shear stresses and the geometric factor associated with the stress/strain relationship in this turbulence model would account for the three-dimensional spreading in a statistical sense. Time-transient liquid jet breakup and ambient gas behavior are computed for an incremental time step (Δt) of 2.5×10^{-6} s. The spray trajectory is tracked in the Lagrangian coordinate system. A different time step that is normally smaller than Δt is applied for this coordinate system. CFD-ACE+ recalculates this time step continuously based on preassigned maximum allowable changes in drop velocity and diameter. The Lagrangian tracking time step, used in the simulations for this study, ranges from 1/3 to 1/10 of Δt. It should be noted that a solution sensitivity study for various numerical parameters, such as grid mesh size, Δt values, etc., was performed prior to obtaining the results of this investigation, as reported in section 5.

Spray tip penetrations from the exit port into the ambient gas for test cases H–1 and H–2 are plotted in figure 18 as a function of time. Predictions from both the Tblob/TTAB and KH/TAB are similar. Nearly straight lines of the tip penetration curves at the beginning indicate that the tip velocity of the liquid jets remains almost constant. Once the jet is fully converted into droplets, the surface area of the spray nose is enlarged and its speed is subsequently reduced, due to greater aerodynamic force and drag. Hence, the penetration curve has a smaller slope at the later time. Furthermore, the results also

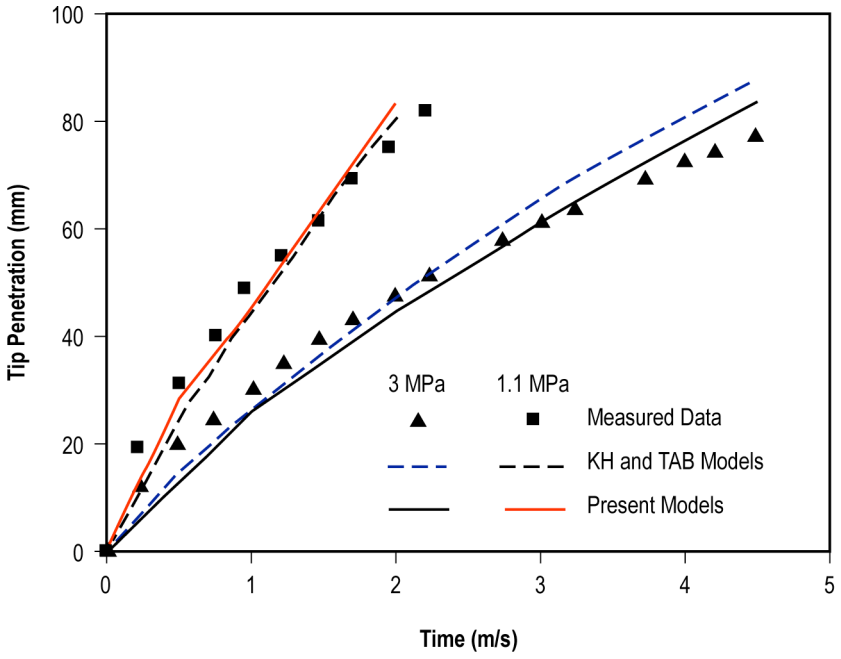

Figure 18. Comparison of measured and predicted spray tip penetrations.

reveal that the spray penetrates at a faster rate into a lower pressure gas. In measurement comparison, tip penetration in both cases is slightly underpredicted at the beginning of the spray with analytical models; however, they are somewhat overpredicted at the later time. Overall, the computational results show close agreement with the experimental data.

Variations in the spray angle due to different ambient gas pressures are depicted in figure 19 for test cases H–1 through H–3. This angle is a global parameter used to characterize the radial expansion of the spray. For an axisymmetric case, as shown in figure 19, the angle is formed by two opposite tangent lines drawn along the spray envelope. The results portray higher backpressure with a larger radial expansion of the spray. Further examination of the atomization modeling suggests that the radial product drop velocity, as estimated from equation (29) of the primary breakup process, is related to the wavelength and its maximum growth rate. The values of these parameters, however, are dependent on the liquid-to-gas density ratio. Consequently, higher gas pressure would result in a larger radial-to-axial velocity ratio and a wider spray angle. In comparison with the results of the KH/TAB models, the present models predict a more favorable, larger spray angle. As stated in section 6.1, the Tblob model estimates considerably larger product drop sizes than the KH model, which leads to the prediction of a stronger radial momentum. Consequently, liquid drops are spread outward more in the Tblob model when compared to the predictions provided by the KH models. As shown in figure 19, a better agreement with the measured data is obtained with the present models.

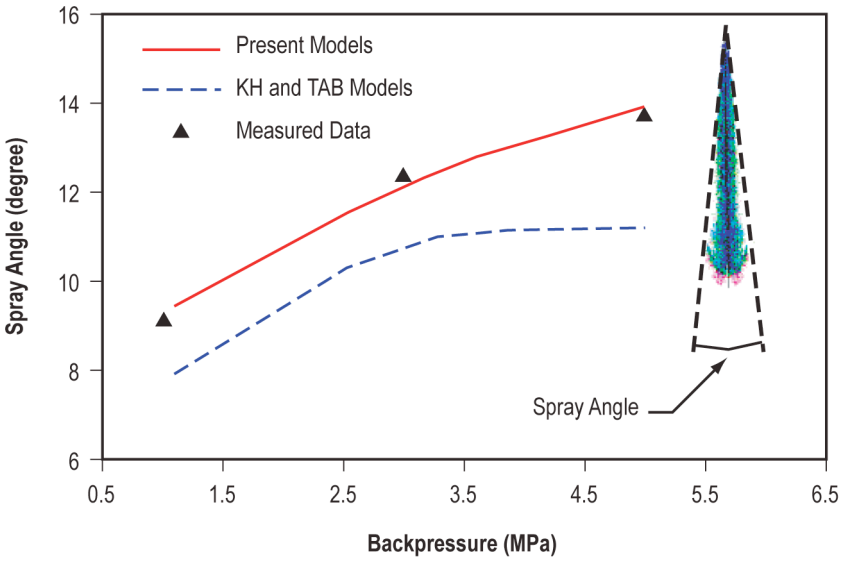

Figure 19. Variations in predicted and measured spray angles at different backpressures.

Computed spray shapes and tip penetrations from the present models for three different backpressure conditions after 2.5 m/s of liquid injection are displayed in figure 20. It should be noted that the injection velocity is higher for a lower backpressure condition. Hence, the spray tip penetrates faster into a lower pressure environment, although the drag increases on the periphery of the spray contour. This phenomenon leads to parcels containing small drops being dragged into the wake behind the tip region, which can be clearly observed in figure 20(a) and (b). It is also interesting to note that larger drops appear on the spray tip as well as on the peripheral regions near the tip. Generally, large drops carry

a stronger momentum that decay less than their smaller drop counterparts. Hence, the large drops tend to travel downstream faster than the smaller drops. In addition, large drops found in these regions may reflect the effect of drop coalescence, which is more pronounced in an elevated gas pressure. As figure 20(c) illustrates, a larger drop size can be observed in the tip region at higher ambient pressures.

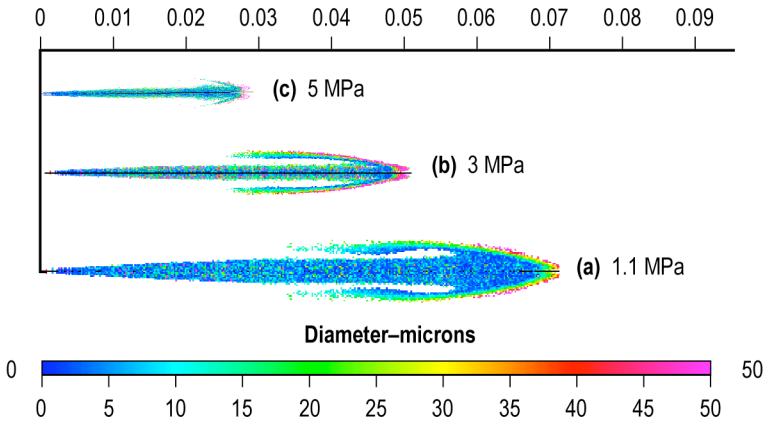

Figure 20. Variations in spray shape, tip penetration, and drop size at $t = 2.5$ m/s due to different backpressures: (a) 1.1 MPa, (b) 3 MPa, and (c) 5 MPa.

Results collected from numerical simulations of test case K are shown in table 1. This test case was selected to evaluate the atomization models because of its available measured drop size data. In the experiment, Koo measured diesel sprays with a phase/doppler particle analyzer (PDPA) system.[48] In general, a PDPA can only recognize a defined range of droplet diameters due to digital processing hardware limitations, as described in the work of Rhys.[55] Normally, the ratio of the largest observable droplet to the smallest observable droplet cannot exceed 35. Regarding this experiment, the instrument was set to measure drop sizes from 1.8 to 246 μm. In this analysis, the same grid mesh and physical domain were used as displayed in figure 5. It should be noted that the liquid fuel injection was driven by a cyclic pumping system for which the mass injection rate is no longer constant. To more realistically simulate the inlet flow conditions, the transient injection velocity profile, reported by Koo and shown in figure 21, was utilized in the computations.

Similar to the previous computational cases, this test case also simulated the transient flow field conditions with $\Delta t = 2.5 \times 10^{-6}$ s. It should be noted that the present simulation utilizes the RANS approach to obtain the mean velocity field of the gas phase. For statistically unstationary flows, which were investigated experimentally by Koo in this case, the interpretation of the averaging process is ensemble averaging.[48,56] Thus, the RANS formulation is justified for the statistically transient case as indicated by the injector inlet condition of figure 21.

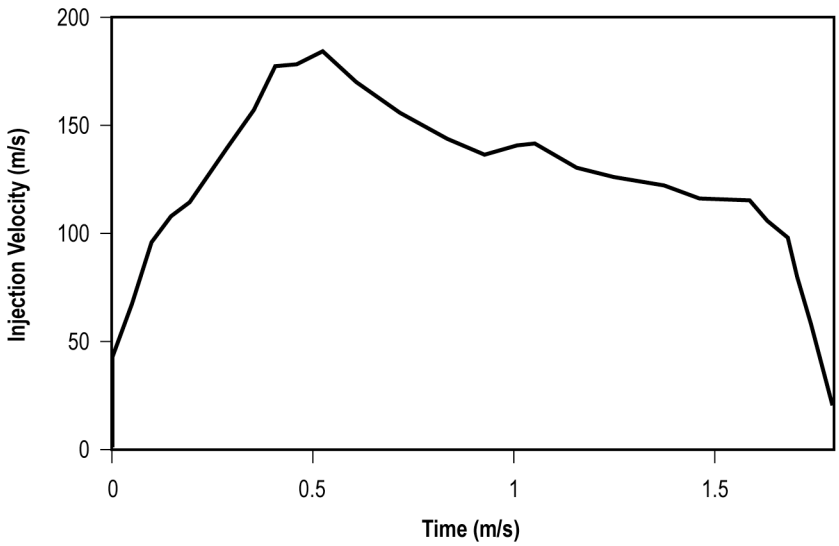

Figure 21. Fuel injection velocity used in simulation for test case K.

The predicted spray tip penetration and the measured data are presented in figure 22. Similar to the computational results obtained from test cases H–1 and H–2, the predictions of this test case, with both the KH/TAB and the present models, are slightly lower than the measurement at the beginning of the injection; however, the predicted curves approach the experimental data at a later time. It is noted that Koo reported the spray penetration length from the beginning of the injection to 1.5 m/s while the computation continues to 3 m/s. In general, both the predicted tip penetrations are similar and their values are in reasonable agreement with the experimental data.

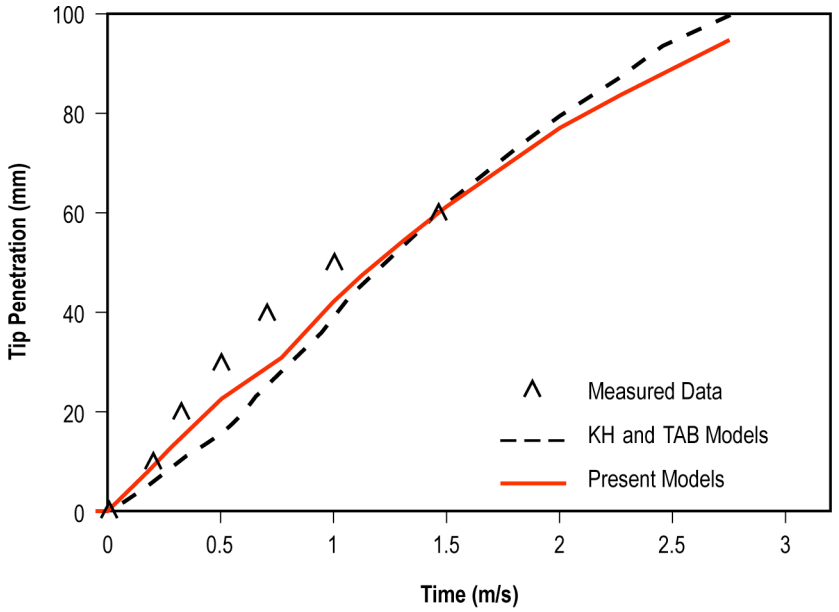

Figure 22. Predicted and measured spray tip penetration for test case K.

Figure 23 displays the simulated spray shapes along with photographs recorded at several time intervals in the experiment. No significant variations appear between the computational results produced for the two sets of atomization models, KH/TAB and Tblob/TTAB. In comparison with the photographs, the simulated spray penetrates into the ambient gas with a slightly shorter distance than the actual distance depicted initially from the photographs; however, the predictions improve significantly afterwards. These results also reflect the same assessment of the tip penetration comparison shown previously in figure 22. It is also interesting to observe the degree of the spray being spread laterally and its tip shape. All the models predict a similar radial expansion of the spray for all considered time intervals and they compare reasonably well with their photographic counterparts. However, the numerical simulations display the tip profile more like a conical shape with parcels containing large drops rather than a round tip as shown in the photographs. Since the momentum of these large drops is degrading much less than the small drops, the large drops move downstream faster than the smaller drops. Therefore, the moving motion of the large drops creates the appearance of the conical shape at the tip. An analysis of the computational cases has been conducted to examine the tip shape variation for different initial spray angles. The analysis suggests that the spray tip head changes to a round shape and does not penetrate into the ambient gas as deeply when increasing the initial spray angle. Tip variation analysis is not addressed in detail here since it is not a main focus in this study.

Further detailed drop size comparisons between the predictions and the measurements are presented in figures 24 and 25. Figure 24(a) reveals the drop sizes recorded at three axial locations along the centerline of the spray. The results indicate that the jet, with an initial diameter of 240 μm, breaks up into relatively large drops along the centerline. Their product drop diameters range from 100 to 200 μm at the stations of $x = 10$ and 20 mm, as shown in figures 24(b) and (c). These results suggest that the primary breakup process is dominant in these regions. Further downstream, the drops undergo the secondary atomization that generates smaller drops. Figure 24(d) exhibits drops of $20 - 50$ μm in diameter at the $x = 60$ mm station. It should also be noted that the fuel injection cycle for this test case is complete at 1.77 m/s; therefore, the drop sizes shown in figures 24(b) and (c) also reflect this end period at which the small drops are registered. The small drops recorded after 1.77 m/s are formed because of the small injection rate at the tail end of the injection cycle, as well as the small drops lagging behind in the spray motion. Generally, predictions from the present models are in good agreement with the measured data. In contrast, the KH and TAB models underpredict the drop size for stations $x = 10$ and 20 mm; however, their predictions are improved significantly at the $x = 60$ mm station. This observation is consistent with earlier results presented in section 6.1. The results also show that the KH model generally predicts smaller drop sizes than the Tblob model.

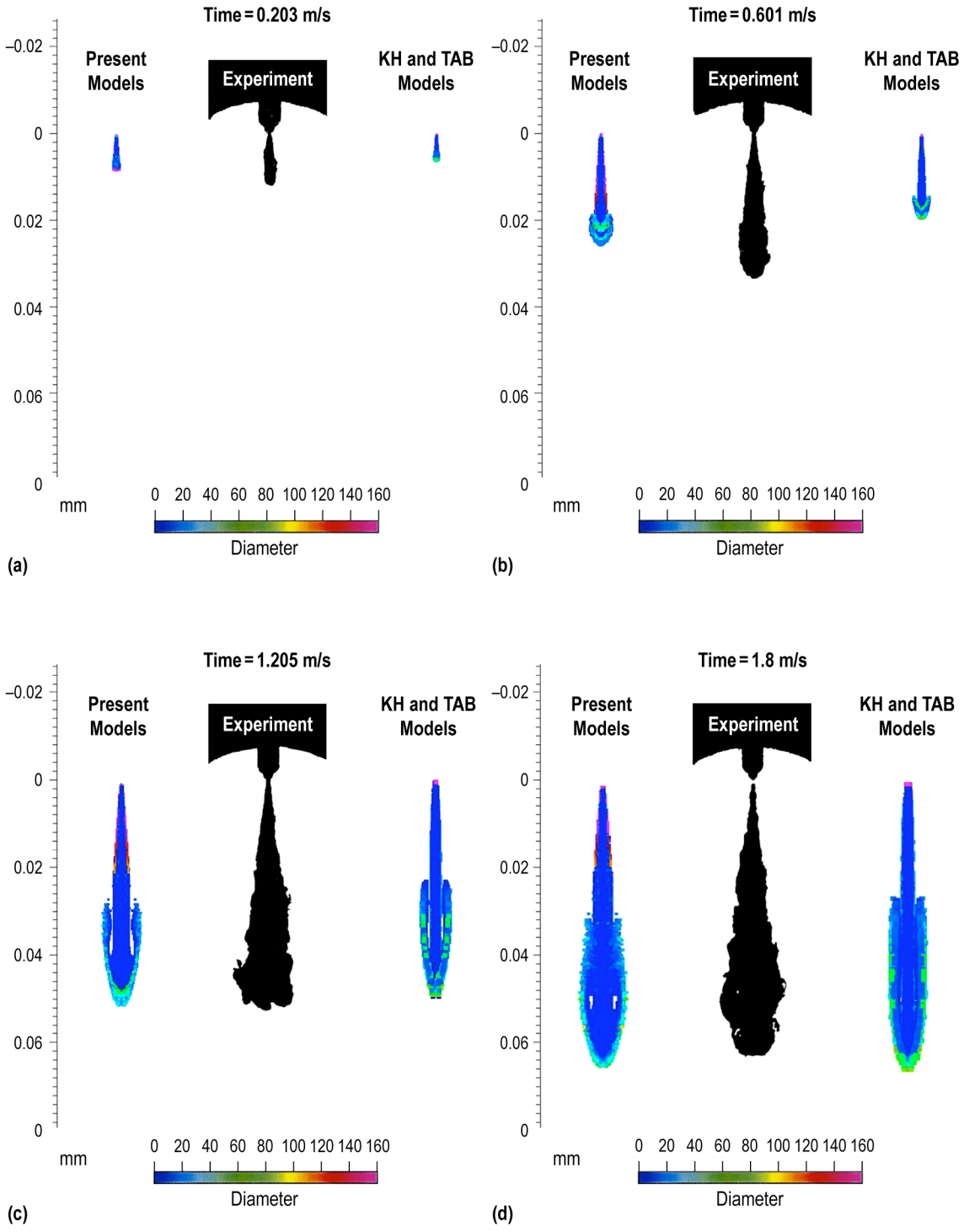

Figure 23. Simulations and photographs of sprays for test case K: (a) At $t = 0.203$ m/s, (b) at $t = 0.601$ m/s, (c) at $t = 1.205$ m/s, and (d) at $t = 1.8$ m/s.

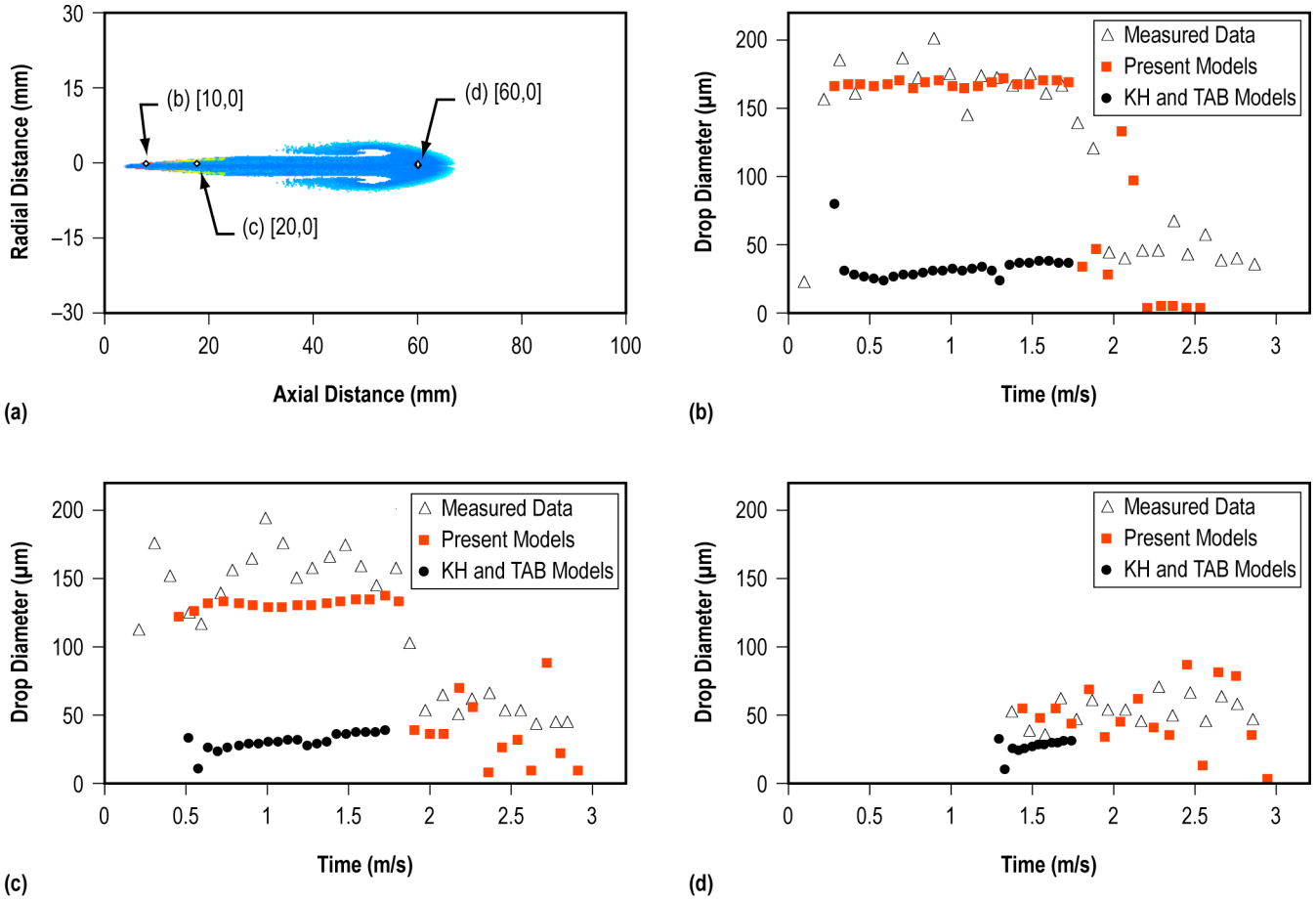

Figure 24. Drop-size distribution from the predictions and measurements for test case K: (a) Coordinates of locations where drops recorded, (b) drop size at [10,0], (c) drop size at [20,0], and (d) drop size at [60,0].

Figure 25(a) displays the drop sizes at three off centerline locations [x,y]. Relatively large drops registered at the [10,0.5] location with diameters ranging from 30 to 180 µm with a random order in time as shown in figure 25(b). Smaller drops are observed after the end of the injection cycle at t = 1.77 m/s, similar to the results shown in figure 24. The present model predictions capture large drops intermittently at certain short time intervals; however, both the KH/TAB and Tblob/TTAB atomization models typically project a much smaller drop size than the measurement portrayed. In other words, the CFD simulation indicates that the secondary droplet breakup process takes place at this location but not the primary breakup. The drop diameter at [10,1.5] and [30,2] varies from 20 to 50 µm, as shown in figures 25(c) and 25(d), respectively. This suggests that considerably smaller drops appear on the spray periphery, and their presence in this outermost region forms the shape of the spray. Furthermore, since the drop sizes at these locations are relatively small, the secondary droplet breakup occurs mostly in these regions. This assessment is consistent with the observation of Koo in his measured data analysis. He concluded that the small droplets in the periphery of the spray are not those directly injected from the nozzle. The small droplets from the nozzle travel much slower than the large droplets that are produced in the primary breakup; hence, they cannot maintain the spray shape observed in the experiments

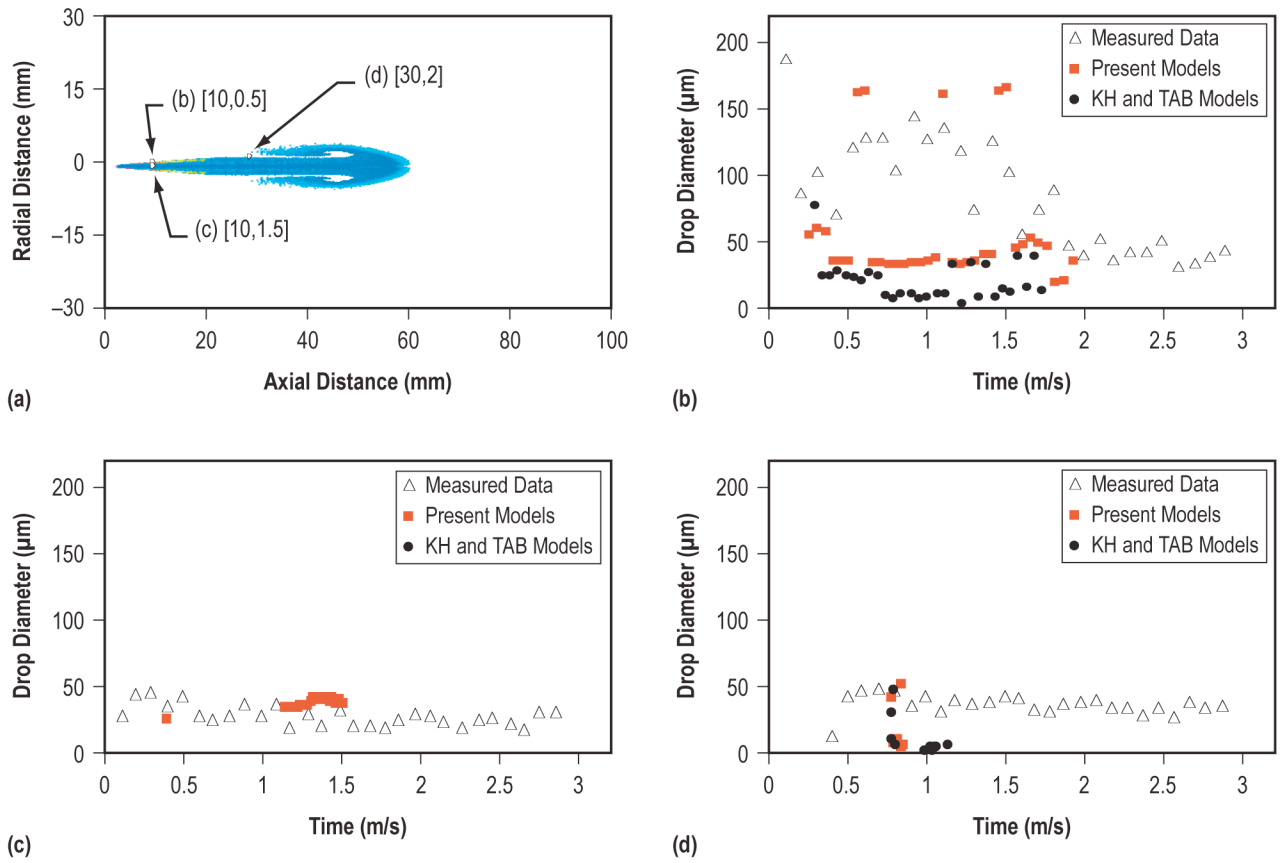

Figure 25. Drop-size distribution from the predictions and measurements for test case K: (a) Coordinates of locations where drops recorded, (b) drop size at [10,0.5], (c) drop size at [10,1.5], and (d) drop size at [30,2].

without the appearance of drops formed by the secondary breakup mechanism. It is interesting to note that the simulation with the KH and TAB models has a limited number of parcels and no parcel tracked at [10,1.5] and [30,2], as shown in figures 25(c) and 25(d), respectively. Again, this examination reconfirms that the spray angle predicted by the classical KH and TAB models is a little smaller than the actual angle, as displayed in figure 18. In the present model, numerical simulation captures droplets at [10,1.5] and [30,2] only in a short timespan, but the predicted drop sizes at this interval are close to the measured data.

7. CONCLUSIONS AND RECOMMENDATIONS

The main effort of this research is to model the effects of turbulence within a cylindrical liquid jet on the atomization process. The present models have been formulated by adding the terms accounting for these effects to the widely used KH and TAB atomization models. Predictions from these new models have been fully evaluated by comparing the results of the existing models and the available measurements. This section summarizes the research effort, reports several findings captured in this study, and offers recommendations for further research on the subject topic.

7.1 Summary

In the course of this study, two existing classical atomization models, the KH instability developed by Reitz and the TAB by O'Rourke and Amsden, have been extended to incorporate terms that account for the turbulence contribution on the liquid breakup mechanism from a phenomenological point of view.[22,23] Subject terms are derived primarily from the physical modeling work of Huh et al. and the collective observations of Tseng et al. from their experimental investigations of the turbulent jet breakup.[27,14] It is important to point out that the present models do preserve the original predictions of these two classical models when turbulence is not present.

For primary atomization, the KH model has been modified to implement the turbulence effect using the characteristic scales method associated with individual physical phenomena. In the proposed Tblob model, the characteristic length and time scales of surface wave perturbation and those of turbulence motion are combined, so their contribution to the breakup mechanism is weighted by means of kinetic energy. The rationale for this approach is that the larger kinetic energy motion has a stronger influence in the liquid breakup process. This has led to modification of the equations predicting the mass rate stripped from the blob drop and the product drop size. It has been observed that initial turbulence quantities play a key role on jet disintegration. Their values are estimated from the geometry and flow conditions of the injection nozzle.

For the secondary droplet breakup event, an additional force term that represents the turbulence effect on droplet surface distortion is incorporated into the TAB governing equations. This force term is composed of the deformation rate of the surface distortion, the dissipation rate of the turbulent kinetic energy, and an empirical constant. The value of this constant rests on the data collected from the measurements of drop breakup in a shock tube. Similar to the Tblob primary atomization, the present secondary droplet breakup model also requires initial turbulence quantities. These values are estimated from the energy conservation of the parent drop and product drops from the primary atomization process. When a drop is created from the secondary breakup, turbulence quantities are determined simply from the turbulence values of their parent drop.

Two separate computer programs have been written to individually assess these new models by comparing the predictions with available experimental data as well as results predicted from their classical model counterparts. The proposed atomization models were implemented into an existing

CFD-ACE+ code for further evaluation. The drop collision and coalescence model of O'Rourke was also incorporated into the CFD-ACE+ code to provide more realistic simulations. The computational results were then compared with the measured data and predictions of the original models. Several conclusions can be drawn from these investigations and are reported in the following section.

7.2 Conclusions

The proposed atomization models have been used to simulate several test cases. The flow conditions are listed in table 1. Close examination of the results, presented in section 6, has led to the following conclusions:

- The primary atomization regime predictions generally show that the intact core length of the turbulent liquid jet is slightly shorter than without the turbulence consideration. In fact, at least in the test cases considered in this study, the combined characteristic scales used in the Tblob model result in a shorter jet breakup time, leading to a shorter intact core as compared to the KH model. These predictions are consistent with the breakup observations of fully developed turbulent liquid jets by the other authors.[8,53]

- When the turbulent liquid jet disintegrates and then forms droplets, as observed by Tseng et al., these drops are generally larger than the drops produced by a nonturbulent jet.[14] The computational results of the present models also reflect this finding, particularly in test case H–3, where the product drop size predicted from the TBlob model is approximately one order of magnitude larger than the KH model.

- In general, turbulence inside the liquid jet affects the primary breakup of the liquid jet. This turbulence is characterized by fluid properties, gas flow conditions, and initial turbulence quantities k_0 and ε_0. In turn, these initial quantities are dependent on the flow conditions and the geometry of the injection nozzle.

- According to the results from the TTAB model, turbulence inside the parent drop also plays a role in the droplet surface wave distortion. Similar to the primary breakup, the level of the turbulence effect on the secondary droplet breakup process depends on its initial turbulence values. However, this turbulence effect is diminished after a few droplet breakup cycles. This is due to turbulence reduction from one generation of drops to the next, based purely on the current assumptions of estimating initial turbulence quantities.

- Close examination of the predicted results for several test cases suggest that the values of the forces participating in droplet deformation vary significantly at the initial time. Aerodynamic and turbulence forces are the strongest among them. However, turbulence force approaches a same order of magnitude as surface tension and viscous damping forces at the breakup time, while the magnitude of the aerodynamic force is still maintained. This observation reconfirms that turbulence has a considerable influence on the secondary breakup when compared with surface tension and viscosity effects. But, aerodynamic force still plays a dominant role in the breakup process also.

- In contrast to the characteristics of liquid jet disintegration, the secondary breakup mechanism produces small drops with a short breakup time when turbulence is considered. The turbulence force term in the present model is constructed to promote droplet surface distortion. That formulation leads to predict a smaller drop size and shorter breakup time than the results obtained from the existing TAB model.

- In general, the CFD simulations are able to capture similar spray structures observed in the experiments. The spray tip penetration lengths as well as the appearance of large drops at the spray tips, as predicted from the two sets of atomization models (KH/TAB and Tblob/TTAB), are comparable to the measured data. However, the KH and TAB models estimate smaller spray angles for test cases H–1 through H–3 than the measurements indicate.

- Drop measurements and predictions from test case K indicate that small drops created from the secondary breakup appear in the outermost regions of the spray. This breakup mechanism is responsible for the radial expansion of the spray and these drops then form the spray profile. On the other hand, drops on the centerline of the spray are relatively large. The appearance of large drops at the spray tips may result from drop coalescence. The strong momentum of large drops allows them to travel ahead downstream.

- In summary, for test case K, the CFD simulation using the KH and TAB models tends to underpredict the drop size of the spray, while it is able to reasonably capture the liquid spray structure. On the other hand, the present models predict comparable drop sizes as seen in the measured data. Overall, the predicted results from the present models do agree reasonably with the experimental data.

7.3 Recommendations

This research effort has offered enhancements on the widely used KH and TAB atomization models by incorporating the turbulence effects. Results from the test cases considered in this investigation indicate that the present models make reasonable predictions in comparison with the available measured data. Nevertheless, the present form of these models may not always provide satisfactory results for all other flow conditions. Hence, to make use of the present models and to further evaluate and improve them, the following recommendations are offered:

- The present models are able to provide global predictions of the atomization process and the spray formation for certain flow conditions. Their results are adequate and useful for most practical engineering applications. Nevertheless, by no means are they able to represent accurate and complete descriptions of physical happenings in the liquid atomization process, since they are based on a semiempirical approach and a phenomenological point of view.

- Reasonable results can be obtained from the present models as long as the flow conditions of interest are similar to the conditions studied in this research. In addition, the solution is dependent on the grid mesh, computational domain size, time step, etc., and should be assessed and anchored, if possible, prior to using the computational results.

- The new models simulating the atomization process are based partially on knowing local flow conditions. In other words, the predicted results also depend on the local flow solutions that are computed

by CFD simulations. Unfortunately, these solutions may vary slightly among CFD numerical schemes. Certain care should be taken when implementing these new improved models into a CFD code. The predictions should be validated adequately with available measured data. It is recommended to simulate several test cases provided in table 1.

- This research provides a basic framework to enhance the atomization models; however, the coefficients used in both the original and the present formulations should be reviewed and reevaluated when used beyond the investigated flow conditions. Recent results from the investigation by Grover et al.[57] may be considered when applying these models to a wide Weber number flow range. Grover et al. proposed to improve the atomization models by changing the subject coefficients according to the considered flow conditions.

- The predicted results of the present models are greatly dependent on initial turbulence quantities. Unfortunately, the current form of the present models only provides a rough estimate of these initial values. To obtain more realistic predictions, a more rigorous estimation of the initial turbulence quantities for individual injection nozzles of interest should be found.

- Finally, the present study indicates that, at least for the test cases investigated, the TAB model predicts smaller drops than anticipated on the secondary breakup. With the inclusion of the turbulence effect, the present TTAB model estimates even smaller drop sizes. The recent study by Lengsfeld et al. suggests that the droplet breakup process could be altered by the presence of neighboring droplets. However, the present form of the models does not take this effect into account. Further studies on this topic are suggested to improve the prediction capability.[58]

APPENDIX A—FORMULATION OF TURBULENCE QUANTITIES

This appendix presents detailed derivations of relations and equations involving the turbulence consideration in the liquid jet atomization process. These equations are referenced throughout this TM. Formulations to determine the initial turbulent kinetic energy and its dissipation rate for use in the primary breakup model are shown. Derivations of the turbulence scale relationships and the product drop-size scale associated with the turbulence are presented. Finally, estimated turbulence values for the test cases used in this study are discussed and listed.

A.1 Initial Turbulent Kinetic Energy

Consider a liquid jet issued from an injection nozzle that has the length (L) and the diameter (D) as shown in figure 26. The outlet-to-inlet contraction area ratio of the nozzle is s. The liquid is injected at a velocity of U.

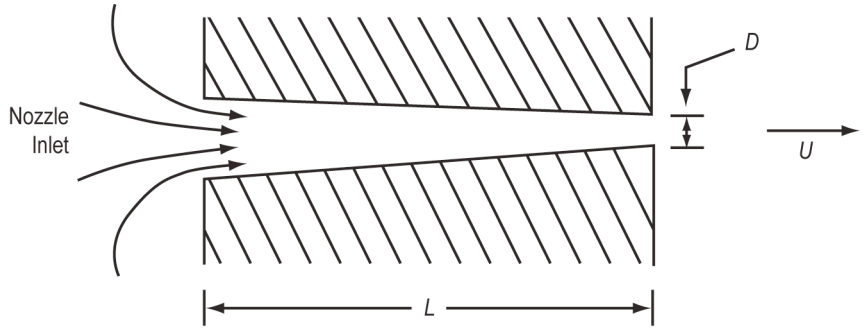

Figure 26. Configuration and flow conditions of a typical injection nozzle.

The total pressure drop (ΔP_{tot}) of the injection nozzle is composed of three components: (1) The pressure drop associated with the nozzle entrance shape (ΔP_{form}), (2) the flow acceleration pressure drop (ΔP_{acc}), and (3) the pressure drop due to the wall shear stress (ΔP_{noz}):

$$\Delta P_{tot} = \Delta P_{form} + \Delta P_{acc} + \Delta P_{noz} \quad . \tag{60}$$

The total pressure drop is expressed in terms of the nozzle discharge coefficient (C_d) as

$$\Delta P_{tot} = \frac{\rho_l U^2}{2C_d^2} \quad . \tag{61}$$

Depending on the shape of the entrance corner, the pressure drop occurs when the fluid enters into the nozzle and can be estimated with a loss coefficient (K_c) as

$$\Delta P_{form} = K_c \frac{\rho_l U^2}{2} \quad . \tag{62}$$

For a contracting nozzle, the fluid is accelerated due to the reduction of the cross-sectional area from the nozzle inlet to its outlet. The pressure drop associated with the flow acceleration process is estimated as

$$\Delta P_{acc} = \left(1 - s^2\right) \frac{\rho_l U^2}{2} \quad . \tag{63}$$

When substituting the proper terms with equations from (61) to (63) into equation (60), ΔP_{noz} can be calculated as

$$\Delta P_{noz} = \frac{\rho_l U^2}{2C_d^2} - \left(1 - s^2\right) \frac{\rho_l U^2}{2} - K_c \frac{\rho_l U^2}{2} \quad . \tag{64}$$

For a fluid flowing through the injection nozzle, Huh et al. approximated the average turbulent stress by setting it equal to the wall shear stress[27]

$$\rho_l u^2 \pi D L = \Delta P_{noz} \frac{\pi D^2}{4} \quad . \tag{65}$$

The parameter (u^2) is the square of the turbulent fluctuation velocity. After placing equation (65) into equation (64), the initial turbulent kinetic energy (k_t^0) can be calculated as

$$k_t^0 = u^2 = \frac{U^2}{8\,L/D} \left[\frac{1}{C_d^2} - K_c - \left(1 - s^2\right) \right] \quad . \tag{66}$$

A.2 Initial Dissipation Rate of Turbulent Kinetic Energy

To determine the initial dissipation rate of the turbulent kinetic energy, Huh et al. assumed that the dissipation rate is proportional to the work done by ΔP_{noz} on the nozzle volume as follows:[27]

$$\varepsilon_t^0 \left[\rho_l \frac{\pi D^2 L}{4} \right] = K_\varepsilon \Delta P_{noz} \left[\frac{\pi D^2}{4} \right] L \left[\frac{U}{L} \right] \quad . \tag{67}$$

The average dissipation rate of the initial turbulent kinetic energy is represented by ε_t^0 . The proportionality constant (K_ε) is found equal to 0.23 by comparing it with multidimensional internal

nozzle flow calculations.[59] By substituting ΔP_{noz} in the equation above with equation (64), ε_t^0 can be expressed as

$$\varepsilon_t^0 = K_\varepsilon \frac{U^3}{2L}\left[\frac{1}{C_d^2} - K_c - \left(1 - s^2\right)\right] . \tag{68}$$

A.3 Derivation of Turbulence Scales

It should be noted that the internal turbulence of the parent drop decays with time as it travels downstream. Assuming a homogeneous isotropic turbulence with no internal turbulence generation, the well-known k-ε turbulence model can be written in terms of the time derivatives of the turbulent kinetic energy (k) and its dissipation rate (ε) as

$$\frac{dk}{dt} = -\varepsilon \tag{69}$$

and

$$\frac{d\varepsilon}{dt} = -C_\varepsilon \frac{\varepsilon^2}{k} . \tag{70}$$

The k-ε turbulence constant (C_ε) is equal to 1.92. The equations above do not account for the effects of the parent drop breakup process and collision/coalescence to the drop internal turbulence. Huh et al. were able to obtain an analytical solution of the k-ε equation model for the individual parent drop as follows: When ε in equation (70) is replaced with dk/dt of equation (69), the relation of the derivatives between k and ε becomes[27]

$$\frac{d\varepsilon}{\varepsilon} = C_\varepsilon \frac{dk}{k} . \tag{71}$$

When integrating equation (71) with the initial conditions of $k(0) = k_t^0$ and $\varepsilon(0) = \varepsilon_t^0$, the solution of ε is

$$\varepsilon = \varepsilon_t^0 \left(\frac{k}{k_t^0}\right)^{C_\varepsilon} . \tag{72}$$

Replacing ε of equation (71) with equation (72), the derivative of k can be expressed as

$$\frac{dk}{k^{C_\varepsilon}} = \frac{\varepsilon_t^0}{\left(k_t^0\right)^{C_\varepsilon}} dt . \tag{73}$$

The turbulent kinetic energy (k) can be obtained by integrating equation (73) over time and with the initial condition of $k(0) = k_t^0$

$$k = \left[\frac{\varepsilon_t^0}{\left(k_t^0\right)^{C_\varepsilon}} \left(1 - C_\varepsilon\right) t + \left(k_t^0\right)^{\left(1-C_\varepsilon\right)} \right]^{1/\left(1-C_\varepsilon\right)} . \tag{74}$$

The turbulence characteristic time and length scales are defined in terms of k and ε as

$$\tau_t = C_\mu \frac{k}{\varepsilon} , \tag{75}$$

$$L_t = C_\mu \frac{k^{3/2}}{\varepsilon} . \tag{76}$$

The parameter (C_μ) is another k-ε turbulence constant and is set equal to 0.09. τ_t and L_t can be expressed as a function of time and initial conditions by performing substitutions of ε and k from equations (72) and (74) into equations (75) and (76):

$$\tau_t = C_\mu \left(C_\varepsilon - 1\right) t + \tau_t^0 \tag{77}$$

and

$$L_t = L_t^0 \left[\frac{C_\mu \left(C_\varepsilon - 1\right) t}{\tau_t^0} + 1 \right]^{\left(\frac{1}{1-C_\varepsilon}\right)\left(\frac{3}{2}-C_\varepsilon\right)} , \tag{78}$$

where

$$\tau_t^0 = C_\mu \frac{k_t^0}{\varepsilon_t^0} \text{ and } L_t^0 = C_\mu \frac{\left(k_t^0\right)^{3/2}}{\varepsilon_t^0} .$$

For $C_\mu = 0.09$ and $C_\varepsilon = 1.92$, equations (77) and (78) become

$$\tau_t = \tau_t^0 + 0.0828t \tag{79}$$

and

$$L_t = L_t^0 \left[1 + \frac{0.0828t}{\tau_t^0} \right]^{0.457} \quad . \tag{80}$$

A.4 Product Drop-Size Scale Associated With Turbulence Motion

In the present primary breakup model, the product drop size is formulated using two unique length scales—surface wave perturbation and turbulence motion. The scale associated with turbulence is derived in the remainder of this appendix.

A.4.1 Governing Equations

Huh et al., represented the diameter of the product drops associated with turbulence motion by a probability density function denoted as $P(d_t)$, where d_t is the diameter of the product drop.[27] This function is proportional to the turbulence energy spectrum and the reciprocal of the time scale. It is based on the notion that an eddy motion with larger kinetic energy and shorter atomization time is likely to appear more frequently as an atomized droplet.

$$P(d_t) = C_p \frac{\Phi(d_t)}{\tau_p} \quad , \tag{81}$$

where $\Phi(d_t)$ is the turbulence energy spectrum given as[56]

$$\Phi(d_t) = \frac{(k/k_e)^2}{\left[1 + (k/k_e)^2 \right]^{11/6}} \quad . \tag{82}$$

The wave number (k) is the inverse of the droplet diameter (d_t) and k_e is obtained from

$$k_e = \frac{1}{L_e} \text{ with } L_e = \frac{L_t}{0.75} \quad ,$$

where L_e is the size of eddies with the maximum energy in the turbulence energy spectrum. The constant (C_p) is determined by the normalization condition

$$\int_{-\infty}^{+\infty} P(x) dx = 1 \quad , \tag{83}$$

where x is a dependent variable of the integral that represents the product drop diameter (d_t).

A.4.2 Product Drop-Size Scale

To calculate the diameter of the product drop, the normalization coefficient (C_p) is evaluated by substituting equations (81) and (82) into equation (83) resulting in

$$\frac{C_p}{\tau_t}\int_{d_{min}}^{d_{max}} \frac{\left(k_e x\right)^{-2}}{\left[1+\left(k_e x\right)^{-2}\right]^{11/6}} dx = 1 \ . \tag{84}$$

It should be noted that the integral in equation (84) is not finite due its infinity limits. Therefore, the limits of the original integral have been changed from $+\infty$ and $-\infty$ to d_{max} and d_{min}. For the current calculation, d_{max} is set equal to the diameter of the injector nozzle (D) while d_{min} is set to10^{-8} m.

Since the product drop size involving the turbulence motion is estimated from the probability density function, as shown in equation (83), the associated radius can be written as follows:

$$r_t = \frac{d_t}{2} = \frac{1}{2}\int_{d_{min}}^{d_{max}} xP\left(x\right)dx = \frac{1}{2}\frac{C_p}{\tau_t}\int_{d_{min}}^{d_{max}} \frac{x\left(k_e x\right)^{-2}}{\left[1+\left(k_e x\right)^{-2}\right]^{11/6}} dx \ . \tag{85}$$

Substituting the ratio C_p/τ_t in equation (85) by its equivalent in equation (84), the diameter of the product droplets can be calculated from the ratio of the following two integrals:

$$r_t = \frac{1}{2}\frac{\int_{d_{min}}^{d_{max}} \frac{x\left(k_e x\right)^{-2}}{\left[1+\left(k_e x\right)^{-2}\right]^{11/6}} dx}{\int_{d_{min}}^{d_{max}} \frac{\left(k_e x\right)^{-2}}{\left[1+\left(k_e x\right)^{-2}\right]^{11/6}} dx} \ . \tag{86}$$

The integrals in the equation above are evaluated with Simpson's composite algorithm.[60]

A.4.3 Initial Turbulence Quantities

For the Tblob primary breakup model, the initial turbulent kinetic energy and its dissipation rate are required. These values, which are estimated from equations (66) and (68), need injection velocity, nozzle geometry, and nozzle flow parameters as shown in table 2. This table lists values of subject quantities used in the test cases and stated in section 5. The test case numbers are labeled in the same way as shown in table 1. Several values in this table are assumed and/or estimated due to unavailable measured data in some experiments. These are denoted by a footnote under the table.

Table 2. Parameters of test cases for estimating turbulence quantities.

Case	H–1	H–2	H–3	Y–1	Y–2	Y–3	K	S
Nozzle diameter, D_{inj} (mm)	0.3	0.3	0.3	0.213	0.213	0.213	0.24	0.15
Nozzle length, L (mm)	0.8[a]	0.8[a]	0.8[a]	0.67	0.67	0.67	0.8	0.8[a]
Discharge coefficient, C_d	0.7[b]	0.7[b]	0.8[b]	0.6	0.6	0.6	0.67	0.7[b]
Entrance loss coefficient, K_c	0.45[c]	0.45[c]	0.45[c]	0.45[c]	0.45[c]	0.45[c]	0.45[c]	0.45[c]
Injection throat/exit area ratio	0[d]	0[d]	0[d]	0.01	0.01	0.01	0.01	0[d]
Injection velocity (m/s)	115.8	102.54	86.41	185.42	185.42	185.42	133.81	183.0021
Initial Turbulence Quantity								
Kinetic energy (m^2/s^2)	2.88×10^2	2.26×10^2	3.94×10^1	1.58×10^3	1.58×10^3	1.58×10^3	5.22×10^2	4.64×10^2
Dissipation rate of kinetic energy (m^2/s^3)	1.06×10^8	7.34×10^7	1.22×10^7	1.49×10^9	1.49×10^9	1.49×10^9	3.14×10^8	6.11×10^8
Authors	Hiroyasu and Kadota	Hiroyasu and Kadota	Hiroyasu and Kadota	Yule et al.	Yule et al.	Yule et al.	Koo	Schneider
Reference	46	46	46	47	47	47	48	49

[a] Assumed value due to the lack of measured data.
[b] Estimated based on given fuel conditions at the nozzle exit.
[c] Assuming that the injection nozzle has a sharp entrance corner.
[d] For the straight injection tube, without throat.

REFERENCES

1. Lefebvre, A.H.: *Atomization and Sprays*, p. 27, Hemisphere Publishing Corporation, New York, 1989.

2. Faeth, G.M.: "Mixing, Transport, and Combustion in Spray," *Prog. Energy Combust.* Sci., Vol. 13, pp. 293–345, 1987.

3. Crowe, C.T.; Troutt, T.R.; and Chung, J.N.: "Numerical Models for Two-Phase Turbulent Flow," *Ann. Rev. Fluid Mech.*, Vol. 28, pp. 11–13, 1996.

4. De Juhasz, K.J.; Zahn, O.F.; and Schweitzer, P.H.: "On the Formation and Dispersion of Oil Sprays," Bulletin No. 40, Engineering Experiment Station, Pennsylvania State University, University Park, PA, 1932.

5. Schweitzer, P.H.: "Mechanism of Disintegration of Liquid Jets," *J. Appl. Phys.*, Vol. 8, pp. 513–521, 1937.

6. Chen, T.-F.; and Davis, J.R.: "Disintegration of the Turbulent Water Jet," *J. Hyd. Div.*, Vol. 1, pp. 175–206, 1964.

7. Grant, R.P.; and Middleman, S.: "Newtonian Jet Stability," *Am. Inst. Chem. Eng. J.*, Vol. 12, pp. 669–678, 1966.

8. Phinney, R.E.: "The Breakup of a Turbulent Liquid Jet in a Gaseous Atmosphere," *J. Fluid Mech.*, Vol. 60, Part 4, pp. 689–701, 1973.

9. McCarthy, M.J.; and Malloy, N.A.: "Review of Stability of Liquid Jets and the Influence of Nozzle Design," *Chem. Eng. J.* Vol. 7, pp. 1–20, 1974.

10. Wu, P.-K.; Tseng, L.-K.; and Faeth, G.M.: "Primary Breakup in Gas/Liquid Mixing Layers for Turbulent Liquids," *At. Sprays*, Vol. 2, pp. 293–317, 1992.

11. Wu, P.-K.; and Faeth, G.M.: "Aerodynamic Effects on Primary and Secondary Spray Breakup," *At. Sprays*, Vol. 3, pp. 265–289, 1993.

12. Wu, P.-K.; and Faeth, G.M.: "Onset and End of Drop Formation Along the Surface of Turbulent Liquid Jets in Still Gases," *Phys. Fluid A*, Vol. 7, pp. 2915–2917, 1995.

13. Wu P.-K.; Miranda, R.F.; and Faeth, G.M.: "Effects of Initial Flow Conditions on Primary. Breakup of Nonturbulent and Turbulent Round Jets," *At. Sprays*, Vol. 5, pp. 175–196, 1995.

14. Tseng, L.-K.; Wu, P.-K.; and Faeth, G.M.: “High-Speed Multiphase Mixing Layers,” Report No. GDL/GMF–92–02, Department of Aerospace Engineering, University of Michigan, Ann Arbor, MI, Final Report, ONR Grant No. N00014–89–J–1199, August 1992.

15. Sallam, K.A.; Dai, Z.; and Faeth, G.M: ”Liquid Breakup at the Surface of Turbulent Round Liquid Jets in Still Gases,” *Int. J. Multiphase Flow*, Vol. 28, pp. 427–449, 2002.

16. Sallam, K.A.; and Faeth, G.M.: “Surface Properties During Primary Breakup of Turbulent Liquid Jets in Still Air,” *AIAA*, Vol. 41, No. 8, pp. 1514–1524, 2003.

17. Rayleigh, L.: “On the Stability of Jets,” *Proc. London Math Soc.*, Vol. 10, No. 4, 1878.

18. Bogy, D.B.: “Drop Formation in a Circular Liquid Jet,” *Ann. Rev. Fluid Mech.*, Vol. 11, pp. 207–228, 1979.

19. Rangel, R.H; and Sirignano, W.A.: “Nonlinear Growth of Kelvin-Helmholtz Instability: Effect of Surface Tension and Density Ratio,” *Phys. Fluids,* Vol. 31, No. 7, pp. 1845–1855, 1988.

20. Rangel, R.H.; and Sirignano, W.A.: “The Linear and Nonlinear Shear Instability of a Fluid Sheet,” *Phys. Fluids*, Vol. A3, No. 10, pp. 2392–2400, 1991.

21. Clark, C.J.; and Dombrowski, N.: “Aerodynamic Instability and Disintegration of Inviscid Liquid Sheets,” *Proc. Roy. Soc. London*, Vol. A329, No. 1579, pp. 467–478, 1972.

22. Reitz, R.D.: “Modeling Atomization Processes in High-Pressure Vaporizing Sprays,” *At. and Spray Tech.*, Vol. 3, pp. 309–337, 1987.

23. O’Rourke, P.J.; and Amsden, A.A.: “The TAB Method for Numerical Calculation of Spray Droplet Breakup,” SAE Technical Paper 872089, 1987.

24. Tanner, F.X.: “Liquid Jet Atomization and Droplet Breakup Modeling of Non-Evaporating Diesel Fuel Sprays,” *J. Eng., SAE Transc.*, Vol. 106, Sec. 3, pp. 127–140, 1998.

25. Tanner, F.X.: “A Cascade Atomization and Drop Breakup Model for the Simulation of High-Pressure Liquid Jets,” SAE Paper 2003–01–1044, 2003.

26. Nishimura, A.; and Assanis, D.N.: “A Model for Primary Atomization Based on Cavitation Bubble Collapse Energy,” ICLASS 2000, Pasadena, CA, July 16–20, 2000.

27. Huh, K.Y.; Lee, E.J.; and Koo, J.Y.: “Diesel Spray Atomization Model Considering Nozzle Exit Turbulence Conditions,” *At. Sprays*, Vol. 8, pp. 453–469, 1998.

28. Fromm, J.E.: “Numerical Calculation of the Fluid Dynamics on Drop-on-Demand Jets,” *IBM J. Res. Dev.*, Vol. 28, No. 3, 1994.

29. Child, R.E.; and Mansour, N.N.: "Simulation of Fundamental Atomization Mechanisms in Fuel Sprays," AIAA Paper, No. 88–0238, 1988.

30. Shokoohi, F.; and Elrol, H.G.: "Numerical Investigation of the Disintegration of Liquid Jets," *J. Comp. Phys.*, Vol. 71, Issue 2, pp. 324–342, 1987.

31. Liang, P.; and Ungewitter, U.: "Multi-Phase Simulation of Coaxial Injector Combustion," AIAA–30th Aerospace Sciences Meeting and Exhibit, Reno, NV, 1992–0345, January 6–9, 1992.

32. Yang, H.Q.; Przekwas, A.J.; and Chuech, S.G.: "On Satellite Drop Formation in Liquid Atomization," AIAA–1990–1960, 26th SAE, ASME, and ASEE Joint Propulsion Conference, Orlando, FL, July 16–18, 1990.

33. Klein, M.; and Janicka, J.: "Large-Eddy Simulation of the Primary Breakup of a Spatially Developing Liquid Film," ICLASS, Sorrento, July 13–18, Italy, 2003.

34. De Villiers, E.; Gosman, A.D.; and Weller, H.G.: "Large Eddy Simulation of Primary Diesel Spray Atomization," SAE Paper 2004–01–0100, 2004.

35. Leboissetier, A.; and Zaleski, S.: "Direct Numerical Simulation of the Atomization of a Liquid Jet," ILASS-Europe, Zurich, Switzerland, September 2001.

36. Reitz, R.D.; and Bracco, F.V.; "Mechanism of Atomization of a Liquid Jet," *Phys. Fluids*, Vol. 25, No. 10, pp. 1730–1742, October 1982.

37. Soteriou, C.; Andrews, R.; and Smith, M.: "Direct Injection Diesel Sprays and the Effect of Cavitation and Hydraulic Flip on Atomization," SAE Paper 950080, 1995.

38. Chaves, H.; Knap, M.; Kubitzek, A.; Obermeler, F.; and Schneider, T.: "Experimental Study of Cavitation in the Nozzle Hole of the Diesel Injectors Using Transparent Nozzles," SAE Paper 950290, 1995.

39. Schmidt, P.D.; Rutland, J.C.; and Corradini, M.L.: "A Numerical Study of Cavitating Flow Through Various Nozzle Shapes," SAE Paper 971597, 1997.

40. Reitz, R.D.; and Bracco, F.V.: "On the Dependence of Spray Angle and Other Spray Parameters on Nozzle Design and Operating Conditions," SAE Paper 790494, 1979.

41. Jones, W.P.; and Launder, B.E.: "The Prediction of Laminarization With a Two-Equation Model of Turbulence," *Int. J. Heat Mass Trans.*, Vol. 15, pp. 301–304, 1972.

42. Pope, S.B.: *Turbulent Flows*, Cambridge University Press, pp.182–185, 2000.

43. Tennekes, H.; and Lumley, J.L.: *A First Course in Turbulence*, The M.I.T. Press, Cambridge, MA, pp. 248–286, 1972.

44. Chou, W.-H.; Hsiang, L.-P.; and Faeth, G.M.: "Temporal Properties of Drop Breakup in the Shear Breakup Regime," *Int. J. Multiphase Flow*, Vol. 23, No. 4, pp. 651–669, 1997.

45. Liu, A.B.; Mather, D.; and Reitz, R.D.: "Modeling the Effects of Drop Drag and Breakup on Fuel Sprays," SAE Technical Paper Series 930072, Int. Congress and Exposition, Detroit, MI, March 1–5, 1993.

46. Hiroyasu, H.; and Kadota, T.: "Fuel Droplet Size Distribution in Diesel Combustion Chamber," SAE Paper 740715, 1974.

47. Yule, A.J.; Mo, S.L.; Tham, S.Y.; and Aval, S.M.: "Diesel Spray Structure," ICLASS–85, London, U.K., 1985.

48. Koo, J.-Y.: "Characteristics of a Transient Diesel Fuel Spray," Ph.D. Dissertation, University of Wisconsin-Madison, 1991.

49. Schneider, B.: "Experimental Investigation of Diesel Spray," CRFD and Laser Diagnostic Workshop, 21st CIMAC Congress 1995, Interlaken, Switzerland, May 16, 1995.

50. CFD-ACE+ Theory Manual, CFD Research Corporation, Huntsville, AL, 1997.

51. O'Rourke, P.J.; and Bracco, F.V.: "Modeling of Drop Interactions in Thick Sprays and Comparison With Experiments," *Inst. Mech. Eng.*, pp. 101–116, 1980.

52. Khosla, S.; and Crocker, D.S.: "CFD Modeling of the Atomization of Plain Liquid Jets in Cross Flow for Gas Turbine Applications," GT2004–54269, ASME IGTI Turbo Expo 2004: Combustion and Fuels, Vienna, Austria, June 2004.

53. Yue, Y.; Powell, C.F.; Poola, R.; Wang, J.; and Schaller, J.K.: "Quantitative Measurements of Diesel Fuel Spray Characteristics in the Near-Nozzle Region Using X-Ray Absorption," *At. Sprays*, Vol. 11, No. 4, pp. 471–490, 2001.

54. Liang, P.Y.; Eastes, T.W.; and Gharakhari, A.: "Computer Simulation of Drop Deformation and Drop Breakup," AIAA 88–3142, 1988.

55. Rhys, O.N.: "Acoustic Excitation and Destruction of Liquid Sheets," Ph.D. Dissertation, The University of Alabama in Huntsville, Huntsville, AL, pp. 90–91, 1999.

56. Hinze, J.O.: *Turbulence*, 2nd ed., McGraw-Hill, New York, NY, 1975.

57. Grover, R.O.; Assanis, D.N.; and Lippert, A.M.: "A Comparison of Classical Atomization Models Against Current Experimental Measurements Within a Zero-Dimensional Framework," ILASS Americas, 17th Annual Conference on Liquid Atomization and Spray Systems, Arlington, VA, May 2004.

58. Lengsfeld, C.S.; Delplanque, J.D.; and Dunn-Rankin, D.: “Breakup Transitions Within Dense Sprays,” *At. Sprays*, Vol. 12, pp. 501–511, 2002.

58. Huh, K.Y.; and Gosman, A.D.: “A Phenomenological Model of Diesel Spray Atomization,” *Proc. Int. Conf. on Multiphase Flow*, Boston, MA, 1991.

60. Burden, R.L.; and Faires, J.D.: *Numerical Analysis*, 3rd ed., p. 676, PWS Publishers, 1985.

61. Trinh, H.P.: “Modeling of Turbulence Effect on Liquid Jet Atomization,” Ph.D. Dissertation, The University of Alabama in Huntsville, Huntsville, AL, 2004.

REPORT DOCUMENTATION PAGE

Form Approved
OMB No. 0704-0188

1. AGENCY USE ONLY *(Leave Blank)*	2. REPORT DATE	3. REPORT TYPE AND DATES COVERED
	December 2007	Technical Memorandum

4. TITLE AND SUBTITLE

Modeling of Turbulence Effect on Liquid Jet Atomization

5. FUNDING NUMBERS

6. AUTHORS

H.P. Trinh

7. PERFORMING ORGANIZATION NAME(S) AND ADDRESS(ES)

George C. Marshall Space Flight Center
Marshall Space Flight Center, AL 35812

8. PERFORMING ORGANIZATION REPORT NUMBER

M–1213

9. SPONSORING/MONITORING AGENCY NAME(S) AND ADDRESS(ES)

National Aeronautics and Space Administration
Washington, DC 20546–0001

10. SPONSORING/MONITORING AGENCY REPORT NUMBER

NASA/TM—2007–215189

11. SUPPLEMENTARY NOTES

Prepared by the ER 32 Propulsion Systems Dept., Engineering Directorate

12a. DISTRIBUTION/AVAILABILITY STATEMENT

Unclassified-Unlimited
Subject Category 34
Availability: NASA CASI 301–621–0390

12b. DISTRIBUTION CODE

13. ABSTRACT *(Maximum 200 words)*

Recent studies indicate that turbulence behaviors within a liquid jet have considerable effect on the atomization process. Such turbulent flow phenomena are encountered in most practical applications of common liquid spray devices. This research aims to model the effects of turbulence occurring inside a cylindrical liquid jet to its atomization process. The two widely used atomization models—Kelvin-Helmholtz (KH) instability of Reitz and the Taylor analogy breakup (TAB) of O'Rourke and Amsden—portraying primary liquid jet disintegration and secondary droplet breakup, respectively, are examined. Additional terms are formulated and appropriately implemented into these two models to account for the turbulence effect. Results for the flow conditions examined in this study indicate that the turbulence terms are significant in comparison with other terms in the models. In the primary breakup regime, the turbulent liquid jet tends to break up into large drops while its intact core is slightly shorter than those without turbulence. In contrast, the secondary droplet breakup with the inside liquid turbulence consideration produces smaller drops. Computational results indicate that the proposed models provide predictions that agree reasonably well with available measured data.

14. SUBJECT TERMS

liquid jet breakup, liquid jet atomization, atomization model, primary droplet breakup, secondary droplet breakup, turbulence effects, liquid spray model

15. NUMBER OF PAGES

88

16. PRICE CODE

17. SECURITY CLASSIFICATION OF REPORT	18. SECURITY CLASSIFICATION OF THIS PAGE	19. SECURITY CLASSIFICATION OF ABSTRACT	20. LIMITATION OF ABSTRACT
Unclassified	Unclassified	Unclassified	Unlimited

NSN 7540-01-280-5500

Standard Form 298 (Rev. 2-89)
Prescribed by ANSI Std. 239-18
298-102

National Aeronautics and
Space Administration
IS20
George C. Marshall Space Flight Center
Marshall Space Flight Center, Alabama
35812